Attenuation and dispersion of first sound near the superfluid transition of ^{3}He-^{4}He mixtures*

C. Buchal and F. Pobell
Institut für Festkörperforschung, Kernforschungsanlage Jülich, 517 Jülich, West Germany
(Received 26 January 1976)

The attenuation α, the velocity u, and the dispersion $D = u(\omega) - u(0)$ of first sound have been determined in ^{3}He-^{4}He mixtures (molar ^{3}He concentrations $X_3 = 0$, 0.070, 0.194, 0.377, and 0.517) at frequencies $2.3 \leq \omega/2\pi \leq 627$ kHz, and in the temperature range $1\ \mu\text{K} \leq |T - T_\lambda| \leq 10$ mK. From the measured velocities we calculate the thermodynamic velocity $u(0)$, as well as $(\partial S/\partial P)_\lambda$ and $(\partial V/\partial P)_\lambda$. The attenuation and the dispersion are considerably reduced when the ^{3}He concentration is increased. They are interpreted as arising from a relaxation process occurring only below T_λ, and a fluctuation process occurring on both sides of the λ transition. Both contributions have about equal strength. The strength A_R of the relaxation process decreases nearly three orders of magnitude with increasing X_3 in our concentration range. Using the obtained relaxation time $\tau' = \tau'_0 t^{-x'}$ (with $t = |T - T_\lambda|/T_\lambda$), and published data for the correlation length ξ', and for the second-sound velocity u_2, we find $\tau' = \xi'/u_2$ for $T < T_\lambda$. The amplitude τ'_0 increases more than one order of magnitude with increasing X_3 in the investigated concentration range. For $T > T_\lambda$, our absorption and dispersion data for all ω and X_3 can be scaled with functions of $\omega\tau$ over four decades of $\omega\tau$. This scaling analysis shows that the time τ characterizing the critical attenuation and dispersion at $T > T_\lambda$ has the same temperature and concentration dependence as the relaxation time τ' at $T < T_\lambda$; these two times differ at most by a constant multiplicative factor. Below T_λ, the data are represented by the sum of the contribution represented by the scaling function plus the contribution from order parameter relaxation. The frequency dependences of the attenuation and of the dispersion for $\omega\tau \gtrsim 1$ scale as $\alpha \sim \omega^{1+y}$ and $D \sim \omega^y$, respectively, with $y = 0.10$ for $X_3 < 0.2$; the exponent y increases at higher X_3. For $\omega\tau < 0.1$ our data allow the hydrodynamic behavior $\alpha \sim \omega^2$ and $D \sim \omega^2$.

I. INTRODUCTION

Many properties of liquid helium have been investigated with high precision near the superfluid transition of ^{4}He under saturated vapor pressure, under higher pressure, and in ^{3}He-^{4}He mixtures.[1,2] In general the agreement between experimental results and theoretical predictions of scaling,[3] of the concept of universality,[4] and of the renormalization-group theory[5] are very good.[2,6] This statement may not yet be applied to the attenuation α and dispersion D of first sound near T_λ. First there is no comprehensive theoretical description of α and D near the superfluid transition. And second the velocity and attenuation of first sound near T_λ have been investigated experimentally only for pure ^{4}He at saturated vapor pressure, first by Chase,[7] and Barmatz and Rudnick,[8] and then in more detail and with higher resolution in Refs. 9 and 10. Although rather important information about the dynamics near the superfluid transition could be obtained from acoustic investigations, no measurements at higher pressures have yet been performed. For ^{3}He-^{4}He mixtures the attenuation near T_λ is known only qualitatively,[11] and accurate data for the velocity are limited to low frequencies,[12,13] so that sound dispersion cannot be determined. The special interest of studying critical phenomena as a function of ^{3}He concentration X_3 or pressure P results from the fact that these are "inert" variables for the superfluid transition; i.e., they should leave critical exponents and amplitude ratios unchanged.[4,14]

In this paper we report on a detailed study of attenuation and dispersion of first sound in ^{3}He-^{4}He mixtures of various molar ^{3}He concentrations ($X_3 = 0$, 0.070, 0.194, 0.377, and 0.517) in the low-frequency range $2.3\ \text{kHz} \lesssim \omega/2\pi \lesssim 627$ kHz near T_λ ($5\times10^{-7} \lesssim t = |T - T_\lambda|/T_\lambda \lesssim 5\times10^{-3}$).[15,16]

This paper is organized in several sections. Section II contains a short summary of the theoretical predictions for the thermodynamic velocity, the dispersion, and the attenuation of first sound near T_λ. In Sec. III we describe the cryogenic and acoustic apparatus, as well as the experimental procedure. Our apparatus contains two sound resonators. Hence we could take data simultaneously under identical conditions at two different frequencies. Since we used sample heights of 0.5 cm only, our data are much less influenced by gravity than the data from earlier work.[7-13,17,18] High-temperature resolution and homogeneity are obtained by using slow temperature drifts (2 μK/min), or taking data at constant temperature, regulated to within 0.5 μK. Concentration changes due to temperature changes are negligible because the sample is sealed by a cold valve, and the gas volume above the mixture is kept very small.

In Sec. IV we present the data of the sound veloc-

ity, dispersion, and attenuation. We calculate the thermodynamic velocity of sound $u(0)$, $(\partial S/\partial P)_\lambda$, and $(\partial V/\partial P)_\lambda$ for various X_3. Whenever possible, our results are compared to those of other authors.

Section V is the discussion and interpretation of the dispersion D and attenuation α. It is shown that our attenuation data are consistent with the dispersion data and vice versa. At $T < T_\lambda$ both α and D are separated into a relaxation and a fluctuation contribution. It is shown that these processes give contributions of about equal strength, which decrease strongly with increasing ^{3}He concentration. The order-parameter relaxation time $\tau' = \tau_0' t^{-x'}$ for the investigated X_3 is consistent with $\tau' = \xi'/u_2$, increases with concentration, and has a critical exponent $x' = \nu' + w$ (ν' is the critical exponent of correlation length ξ'; w is the exponent of velocity u_2 of second sound).

The concentration and temperature dependences of the maximum relaxation attenuation and dispersion are discussed. The maximum total attenuation, the maximum relaxation attenuation, and the attenuation near T_λ scale with frequency as $\alpha \sim \omega^{1+y}$, with $y = 0.10$ for $X_3 < 0.2$, and y increasing for the higher concentrations. The maximum of the dispersion shows the corresponding frequency dependence, $D \sim \omega^y$. Only for $\omega\tau < 0.1$, where our data are loosing accuracy do they allow the behavior expected for the hydrodynamic regime, $\alpha \sim \omega^2$, and $D \sim \omega^2$.

The data for $T > T_\lambda$ are analyzed with a scaling function of $\omega\tau$. We find, that the critical attenuation, e.g., can be scaled by the function $f_F = \omega\tau/(c + \omega\tau)$ for all investigated ω and X_3, and $10^2 \geq \omega\tau \geq 10^{-2}$ in spite of its strong ω and X_3 dependence. For $T > T_\lambda$ the resulting characteristic time $\tau = \tau_0 t^{-x}$ has the same temperature and concentration dependence as the relaxation time τ' for $T < T_\lambda$. Hence these two times differ at most by a constant multiplicative factor. Consequently, there exists a unique time scale throughout the critical region, as predicted by dynamic scaling. We find $c = (0.506 \pm 0.005)\tau_0/\tau_0'$, independent of X_3, and for all ω in our range. At least for $X_3 < 0.2$ our attenuation data allow equally well the scaling function $\bar{f}_F = (\omega\tau)^{1-y}/[\bar{c} + (\omega\tau)^{1-y}]$, with the same τ and $\bar{c} = (0.55 \pm 0.01)(\tau_0/\tau_0')^{1-y}$. This modified scaling function agrees with hydrodynamics at $\omega\tau \ll 1$ for $\alpha \sim \omega^{1+y}\bar{f}_F$, and $y \neq 0$. In a corresponding analysis it is shown that the dispersion, too, can be scaled at $T > T_\lambda$ for all investigated ω and $X_3 \leq 0.377$.

For $T < T_\lambda$, the data are represented by the scaling function, determined from the data for the fluctuation contribution at $T > T_\lambda$, plus the contribution from order parameter relaxation. A summary and conclusions are given in Sec. VI.

II. THEORY

A. Thermodynamic velocity of sound

The isentropic sound velocity u experiences a sharp dip near T_λ. It has been shown that for $\omega = 0$ this dip resembles the reciprocal specific heat C_p^{-1}, and that $u(0)$ obeys a modified Pippard relation[19] sufficiently close to T_λ for ^{4}He,[8,17] and for ^{3}He-^{4}He mixtures.[12,13] Near T_λ the thermodynamic relation between u in the zero-frequency limit and the heat capacity C_p is given to a very good approximation[8,12,13,17] by

$$u(0) = aC_p^{-1} + bt + c\,, \tag{1}$$

with $a = (u_\lambda^3 T_\lambda/2V_\lambda^2)(\partial S/\partial P)_\lambda^2$ and $t = |T - T_\lambda|/T_\lambda$. The subscript λ denotes values at the λ temperature. In the limit $T \to T_\lambda$, Eq. (1) becomes thermodynamically exact. The specific heat C_p dominates the behavior of the thermodynamic velocity of sound near T_λ.[8,12,13,17] Because the peak of C_p decreases with increasing X_3,[20] the minimum of u becomes weaker with increasing X_3. Our experimental path is at constant pressure and ^{3}He concentration; we also use parameters from other authors taken along this path if needed in the analysis. We do not perform a renormalization to a path of constant chemical potential difference.

B. Dispersion and attenuation of sound

At finite frequencies the velocity becomes frequency dependent, and a pronounced increase in the sound attenuation occurs near T_λ.[7-11,16] Whereas the early data lacked sufficient precision and temperature control for a detailed comparison to theory,[18] recently detailed studies of sound attenuation α,[9] and dispersion D,[10] have been performed for ^{4}He near T_λ. The results of these experiments have been discussed in terms of attenuation and dispersion arising from two processes.

1. Order-parameter relaxation

This process, first studied by Landau and Khalatnikov,[21] arises because the superfluid density ρ_s needs a relaxation time τ' to reach equilibrium if a pressure wave travels through the liquid. The time τ' increases strongly for $T \to T_\lambda$. Later on,[22] this process has been ascribed to a linear coupling of first and second sound. The relaxation occurs only below T_λ, where the time average of the order parameter is nonzero. If a nonequilibrium order parameter decays exponentially in time with a single relaxation time τ', the resulting attenuation α_R and dispersion D_R are given by

$$\alpha_R = \frac{\Delta u}{u^2}\,\frac{\omega^2\tau'}{1+\omega^2\tau'^2}\,,$$
$$D_R = \Delta u\,\frac{\omega^2\tau'^2}{1+\omega^2\tau'^2}\,, \tag{2}$$

with

$$\tau' = \xi'/u_2 = \tau_0' t^{-\nu'-w} = \tau_0' t^{-x'}$$

(ξ' is the correlation length; u_2 is the velocity of second sound).[21-23] We use primed parameters at $T<T_\lambda$; unprimed parameters are used at $T>T_\lambda$, if they pertain to both phases, or in obvious cases. The difference $\Delta u = u(\infty) - u(0)$ of the velocities in the high- and low-frequency limits has been calculated for ^{4}He,[22,23] as

$$\Delta u = \frac{u^3(0)\rho k_B T}{4\pi\xi'^3}\left[\frac{\rho}{\rho_s}\,\frac{\partial(\rho_s/\rho)}{\partial T}\,\frac{T}{C_p}\left(\frac{\partial S}{\partial P}\right)_\lambda\right]^2. \tag{3}$$

The temperature dependence of Δu, which mostly has been neglected,[8,9,17,18] is then given by

$$\Delta u = A_R t^{3\nu'-2} C_p^{-2}\,, \tag{4}$$

where ν' is the critical exponent of the correlation length, and A_R is a constant. Using the value $3\nu'-2=0.026$ determined recently for ^{4}He,[6] and published values for C_p of ^{4}He,[24] one finds that Δu changes by about 50% per decade of t in our temperature range.[10] Both, α_R and D_R vanish at T_λ. Very recently, Sanikidze has calculated α_R and D_R for ^{3}He-^{4}He mixtures.[25] He also obtains Eqs. (2) and (4) with

$$A_R = \frac{\hbar^2\rho^2 k\zeta^2}{4m^2u(0)\xi_0'^2}\left(\frac{\partial S}{\partial P}\right)_\lambda^2\left[\left(\frac{\partial\rho}{\partial P}\right)_\lambda + \rho^2\left(\frac{\partial S}{\partial P}\right)_\lambda\left(\frac{\partial T}{\partial P}\right)_\lambda - \rho^2\left(\frac{\partial S}{\partial P}\right)_\lambda^2\left(\frac{\partial S}{\partial T}\right)_P^{-1}\right]^{-2}, \tag{5}$$

where k and ζ are the amplitude and critical exponent of ρ_s/ρ near T_λ.[6,26] This relation for A_R may be transformed to Hohenberg's result for A_R [see Eqs. (3) and (4)] by using $\rho_s\xi'/T = \text{const}$.[27-31] Hence Hohenberg's Eq. (3) is valid for the mixtures, too, and the asymptotic temperature behavior of Δu is the same for all X_3. We have

$$\alpha_R = A_R C_p^{-2} t^{3\nu'-2} u^{-2}\omega\,\frac{\omega\tau_0' t^{-x'}}{1+\omega^2\tau_0'^2 t^{-2x'}} = A_R C_p^{-2} t^{3\nu'-2} u^{-2}\omega F_R(\omega\tau)\,,$$
$$D_R = A_R C_p^{-2} t^{3\nu'-2}\,\frac{\omega^2\tau_0'^2 t^{-2x'}}{1+\omega^2\tau_0'^2 t^{-2x'}} = A_R C_p^{-2} t^{3\nu'-2}\omega\tau F_R(\omega\tau)\,, \tag{6}$$

with A_R, C_p, u, τ_0', $3\nu'-2$, and possibly x' depending on ^{3}He concentration[32] (cf. Table I).

Equations (2) or (6) cannot describe the total attenuation and dispersion, because even for $\Delta u = \text{const}$, $\alpha_R \to 0$ for $t \to 0$. Experiments show that α is nonzero at T_λ, and that the proposed minimum of α near T_λ (Fig. 5 of Ref. 18) clearly is absent. Other processes are significantly contributing to attenuation and dispersion near T_λ.

2. *Order-parameter fluctuations*

There is a coupling of the sound wave to critical fluctuations of the order parameter. This occurs on both sides of T_λ, is nonsingular at T_λ, and has been discussed for the superfluid transition in several papers.[23,27,33,34] The contributions from fluctuations above and below T_λ are expected to be about equal for the same values of t, and to be of about the same strength as the relaxation contribution.[23] Kawasaki has obtained the most detailed information by considering a sound wave which interacts with order-parameter fluctuations.[34] Using mode-mode coupling and scaling ideas he derived the following general scaling law form for the sound attenuation near the critical temperature

$$\alpha_F = A_F C_v^{-2} t^{3\nu-2} u^{-2}\omega F_F(\omega\tau)\,,$$

with (7)

$$A_F = k_B T\left(\frac{\partial P}{\partial T}\right)_v^2 \Big/ \rho^3 u\,\xi_0^3\,.$$

Here $\tau = \tau_0 t^{-x}$ is the time characterizing the critical order-parameter dynamics. Of course, the particular scaling functions for the relaxation and for the fluctuation mechanisms, as well as in the superfluid and in the normal-fluid phases can be rather different. For example, F_F should not show the strong decrease at large $\omega\tau$ as F_R does; experimental results indicate that α_F must become rather weakly dependent on t near the transition. However, we expect the critical exponents to be identical in either case. The temperature dependence of Eq. (7) is mainly contained in the scaling function $F_F(\omega\tau)$; the factors in front of F_F are only very mildly dependent on t. Consequently we may write

$$\alpha_F = B_F t^s \omega F_F(\omega\tau) = C_F\omega^{1+s/x} f_F(\omega\tau)\,, \tag{8}$$

where B_F and C_F are constants. We have $s/x \gtrsim 0$, because s is a small positive number. The validity of Eqs. (7) and (8) is restricted to the range where the sound wavelength is much greater than the range of correlation of critical fluctuations ($\omega\tau \ll u/u_2$).[34] This condition is always fulfilled for our measurements. At higher frequencies other processes should contribute which may exceed the discussed contributions.[34-39]

TABLE I. Parameters used in the analysis.

X_3 [a]	0.000	0.070	0.194	0.377	0.517
T_λ (K)	2.172	2.072	1.883	1.556	1.255
$\zeta = \nu'$ (from Refs. 6, 26, and 31) [b]	0.675	0.675	0.675	0.675	0.720
$3\nu' - 2$ (see Ref. 32)	0.026	0.026	0.026	0.026	0.160
w (from Ref. 26)	0.387	0.387	0.388	0.394	0.401
$x' = \nu' + w$	1.062	1.062	1.063	1.069	1.122
$2\alpha'\varphi(t)$ [c]	0.131	0.098	0.052	0.013	0.003
$(\omega\tau')$ at $\alpha_{R,\max}$ [c]	0.86	0.89	0.93	0.96	0.97

[a] These values were determined from the measured $T_\lambda(X_3)$ and the data of Ref. 11.
[b] According to Refs. 26 and 31, $\nu' = \zeta = \text{const}$ for $X_3 < 0.4$, and $\zeta(0.517) - \zeta(0.4) = 0.045$. For $X_3 < 0.4$, we take the value $\zeta = 0.675$ recently determined for ^{4}He (Ref. 6).
[c] Calculated at $t = 10^{-5}$; $(\omega\tau')$ at $\alpha_{R,\max}$ is rather insensitive to t, with a change of less than 3% per decade of t, α' is the critical exponent of the specific heat.

3. *Hydrodynamic regime*

In the hydrodynamic regime ($\omega\tau \ll 1$) all processes and therefore the total attenuation and dispersion above and below T_λ should vary as[1,23]

$$\alpha \sim \omega^2 \quad \text{and} \quad D \sim \omega^2. \tag{9}$$

This has to be fulfilled by Eqs. (7) and (8), therefore, e.g., $f_F(\omega\tau) \sim \omega^{1-s/x}$ for $\omega\tau \ll 1$.

III. EXPERIMENTAL

A. Cryogenics

The essential parts of our cryogenic apparatus are shown in Fig. 1. We have a vacuum can which is surrounded by a ^{4}He bath at $T = 4.2$ K. Lower temperatures are obtained by a continuously operating ^{4}He refrigerator inside the vacuum can.[40] The refrigerator is filled with liquid helium from the bath through an impedance, and pumped through an orifice of $d = 0.1$ cm. Its temperature of about $T = 1.4$ K is regulated to within 10 μK by a thermometer and a heater in an electronic feedback loop.[6,30] All wires, capillaries, and the tubes for a cold valve are carefully heat sunk first at 4.2 K at the top flange of the can, and then at 1.4 K at the refrigerator before they are connected to the sample chamber. The sample chamber inside of the vacuum can is a copper cell of 1 cm minimum wall thickness to ensure temperature homogeneity. Two sound resonators, to be discussed below, are fit tightly into the sample chamber. In addition, a germanium thermometer[41] is fit with grease into a hole in the chamber's wall, and a heater is wound around the wall.

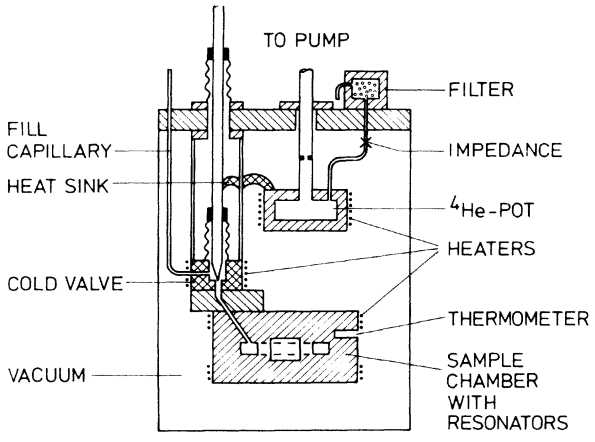

FIG. 1. Cryogenic part of the experimental apparatus.

The cold valve is operated mechanically from room temperature. The two stainless-steel tubes leading to its german-silver seat (0.1-cm-diam hole), and to its stainless-steel needle (3° taper) are well heat sunk by copper braids to the ^{4}He refrigerator, half-way between the top flange of the can and the sample chamber. The seat of the cold valve is bolted to the sample chamber. The weak thermal coupling (40 μW/K) between the sample chamber and the refrigerator is provided via the tubes of the cold valve. A constant heat input to the heater at the cold valve is providing most of the energy to raise the sample temperature above the refrigerator temperature.

B. Resonators

Two first sound resonators suitable for different frequency ranges were fit inside the sample chamber. Both were made out of copper for temperature and therefore concentration homogeneity of

the mixtures. Everywhere in the sample chamber and in the resonators the liquid is at most 0.25 cm away from copper, thus reducing thermal relaxation times. The resonator heights were only 0.5 cm to avoid corrections due to gravity at $t > 10^{-6}$ (see below).[17,18,42] In both resonators, sound was excited and detected by condenser transducers with aluminized Mylar as active elements.[8] The main advantage of these transducers for the present investigation is their good response at low frequencies and their low heat production, a necessity for temperature and concentration homogeneity within mixtures. One resonator was a cylinder[8,10,30,31] (0.5 cm high, 0.8 cm diam) with a fundamental plane-wave harmonic of 21 kHz in ^{4}He; it was used up to frequencies of 630 kHz.[15] The second cavity was a torus (3.0 cm mean diam, 0.3 cm wide; 0.3 cm high), as used by Kojima *et al.*[43] for studies of fourth sound. Its fundamental azimuthal resonance is at 2.3 kHz for ^{4}He. The torus covered the frequency range up to 40 kHz, and in addition served as an "acoustic thermometer" for localizing the λ temperature[10] (see below). The transducers in both resonators were biased with 270 V_{dc}. The ac-drive voltage was about 0.5 V_{rms} for the cylinder, and about 3 V_{rms} for the torus, giving pickup signals of approximately 0.01–1 mV_{eff}, and 1–10 μV_{eff}, respectively, depending on temperature and selected harmonic. First sound could be generated and detected simultaneously in the two resonators at two frequencies with different electronic setups (see below). This method allowed various cross checks.

C. Thermometry

Our main thermometer was a commercial germanium resistor,[41] calibrated against the 1958 ^{4}He-vapor-pressure scale.[44] Its resistance was measured in an ac-bridge arrangement as described in Refs. 6 and 30. The heat (about 1 nW) dissipated in the thermometer resulted in negligible self-heating. Temperature changes of 0.5 μK could be resolved, and the temperature of the copper sample chamber was regulated to within this limit, with the thermometer and the heater (wound around the chamber walls) in an electronic feedback loop[6,30] (heating power during regulation: 5 ± 2 μW). Even for ^{4}He, no anomaly in the thermometer characteristic could be detected while drifting through T_λ, indicating that temperature gradients in the system could at most be of the order of our temperature resolution. With a mixture in the sample, no anomaly is expected anyway, because its thermal conductivity varies smoothly through T_λ.[45] We used the behavior of the velocity of sound near T_λ as an indicator of the superfluid transition.[10] Because of the gravitational pressure gradient in a liquid sample of finite height h, the λ transition occurs at the top of the sample at a temperature T_λ^s which is higher by $ghp(\partial T/\partial P)_\lambda$ than the λ transition at the bottom of the sample[42] [$(\partial T/\partial P)_\lambda$ is the slope of the λ line]. When drifting the sample through T_λ, the sound velocity at zero frequency shows an inflection point at T_λ^s, when the transition reaches the top of the cell.[17] With increasing frequency this inflection point occurs at slightly lower temperatures T_i, as shown in Fig. 2 for $X_3 \leq 0.377$. At $X_3 = 0.517$, the behavior of the sound velocity is more complex (see Fig. 4), and we find the inflection point only at $\omega/2\pi \leq 40$ kHz. For $\omega/2\pi \leq 10$ kHz, $|T_i - T_\lambda^s|$ is less than our resolution of ± 0.5 μK for all investigated mixtures. During every run, we used the torus resonance at $\omega/2\pi \simeq 9$ kHz to determine T_i, set $T_\lambda^s \equiv T_i(9\text{ kHz})$, and refer all our temperatures to this value. For the mixtures we consider this at present to be the most reliable method of determining T_λ. Usually, T_λ has been a free variable parameter in the analysis of data for critical phenomena in ^{3}He-^{4}He mixtures.[20] Our experimental determination of T_λ removes this additional parameter from the analysis, and therefore reduces the uncertainties for the remaining ones.

In searching for possible temperature or concentration differences between the two resonators we recorded the attenuation and velocity of sound with both resonators at about the same frequency (21 or 42 kHz) and drifted in temperature. From

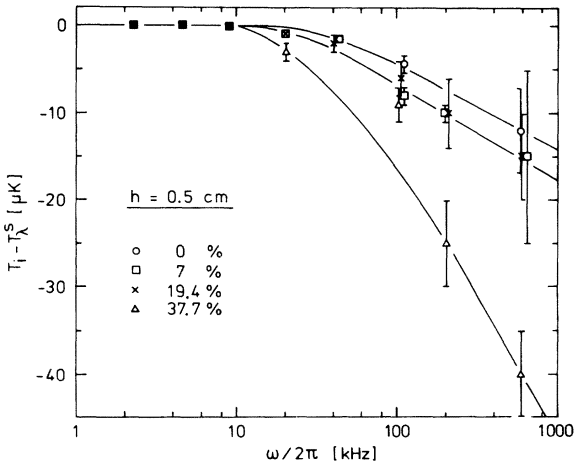

FIG. 2. Temperature difference $T_i - T_\lambda^s$ as a function of sound frequency for the indicated ^{3}He-^{4}He mixtures. Here T_i is the temperature where the velocity of sound has its inflection point (see Fig. 4); T_λ^s is the temperature when the λ transition reaches the top of our 0.5-cm-high sample. The full lines are guides for the eye only.

these checks, as well as taking our resolution in temperature, and the drift of our thermometer (less than 5 μK in 2 weeks) into account, we believe our determination of $|T_\lambda^s - T|$ to be accurate to somewhat better than 1 μK.

D. Electronics for acoustic measurements

In Fig. 3 we show the electronic setup for one resonator. The wave analyzer is operating in the "tracking-generator" mode. It produces a sine wave of tunable frequency ω to drive the resonator, and measures the amplitude of the received signal. The input and output are internally tuned to the same frequency ω, but there is no rigid phase relation between them, i.e., the output is not the filtered input signal. Hence, the resonator is determining the phase relation between the drive and the pickup signal. When tuning through a resonance, the phase changes by 180°. This rapid phase change at ω_0 is used to control the operating frequency. For this purpose a phase-sensitive measurement of the pickup signal, referenced to the drive, is performed. The lock-in amplifier shows a zero out-of-phase signal when the resonator is operated exactly at the resonance frequency ω_0, but small changes $\pm d\omega$ produce a large out-of-phase signal $\pm dV$. The error voltage $\pm dV$ is used to tune the voltage-controlled oscillator back to ω_0. The stability of this arrangement is determined only by the sound resonator and it very sensitively tracks all velocity-of-sound changes. Any instabilities of the oscillator are eliminated by the lock-in amplifier. The system may be locked to any point of the phase curve of the resonator. To measure the quality factor Q of the resonators, it therefore is not necessary to interrupt the advantageous feedback operation. One simply changes the phase setting of the lock-in amplifier, until the amplitude reaches the −3-dB points [$A = A(\omega_0)/\sqrt{2}$; $\varphi = \varphi(\omega_0) \pm 45°$; $\omega = \omega_0 \pm \frac{1}{2}\Delta\omega$].

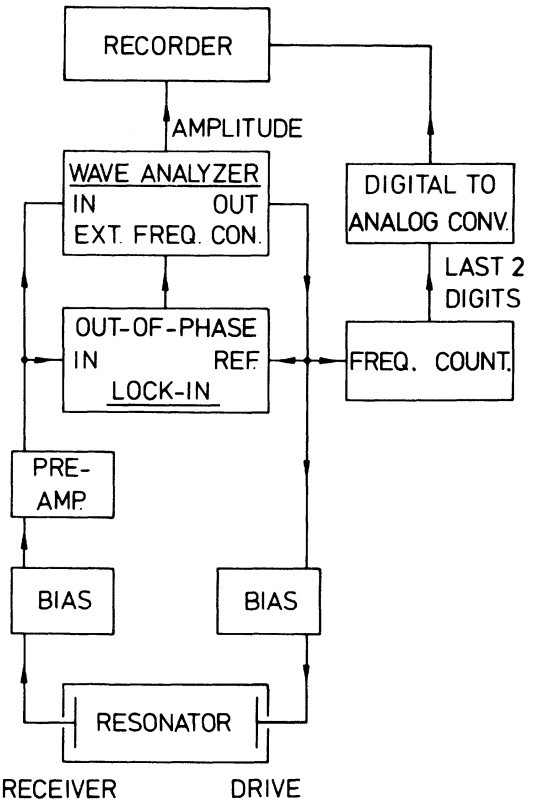

FIG. 3. Electronic setup used for the acoustic investigations.

When locked to the resonance at ω_0, velocity-of-sound changes of $\Delta u/u = 10^{-7}$ are easily measured. But this resolution is not the precision of the data. Changing amplitudes of the pickup signal due to the change of sound attenuation with temperature, the capacities to ground, and sometimes resonance behavior of the drive transducer or microphone induce phase changes which can deteriorate the performance of the system. Therefore during a run we frequently checked the tuning by measuring the −3-dB points of the resonance ($\omega_0 \pm \frac{1}{2}\Delta\omega$) and controlling the center frequency ω_0. Taking all these effects into account, our velocity data have maximum errors of 0.5, 0.5, 0.5, 0.2, and 0.1 cm/sec for $X_3 = 0$, 0.070, 0.194, 0.377, and 0.517, respectively.

E. Procedure

The mixture to be investigated was first condensed into a charcoal trap at 4.2 K. After warming the trap to room temperature, the gas had a pressure of 50–100 bar. The pressurized gas was forced through a small capillary into the sample chamber kept at 1.1–1.3 K. This procedure should produce negligible fractionation. Then the cold valve was closed and the fill capillary above the valve evacuated. With the empty fill capillary, the sample is isolated from its surroundings except for the small heat leak via the tubes of the cold valve to the well-regulated refrigerator. Warming the sample to temperatures near T_λ resulted in a small gas volume below the cold valve. The velocity of sound falls rapidly with decreasing pressure and precisely indicates when vapor pressure is reached. All our data are taken at saturated vapor pressure. The concentrations of the mixtures were determined by measuring T_λ^s and using the X_3-vs-T_λ table of Ref. 11. Keeping the gas volume above the liquid very small ensured that the change of the ratio $X_{3,\text{gas}}/X_{3,\text{liquid}}$ resulting

from temperature changes is negligible.

Data were taken either with the temperature held constant to within 0.5 μK, or during drifts of about 2 μK/min. While the temperature drifted, the resonant frequencies of both resonators, one sound amplitude, and the temperature were recorded simultaneously on a four-pen recorder. When the temperature was held constant, the frequencies at the −3-dB points of the particular resonance were also measured. These data give us the Q value and the total absorption, via $Q=\omega_0/\Delta\omega$ (−3 dB), and $\alpha_{\text{expt}}=\omega/2Qu$. Far away from T_λ, our resonators had Q values of 500–5000, depending on resonator, mixture, and frequency, decreasing to 200–800 near T_λ. Comparing the Q values with the pickup amplitudes U of the resonances, we always found that in the investigated temperature range Q is proportional to U. We then used this relation for calculating α_{expt} in the region where the temperature drifted, and the pickup amplitude was recorded continuously to obtain continuous curves for the absorption coefficient. From the measured attenuation α_{expt} we subtracted a constant background attenuation α_B measured far away from T_λ (e.g., at 600 kHz and in ^{4}He, at $|T-T_\lambda|>10$ mK), in order to obtain the attenuation $\alpha=\alpha_{\text{expt}}-\alpha_B$ associated with the transition. The ratio $\alpha_B/\alpha_{\text{expt}}$ was 0.1 for ^{4}He at 600 kHz, and increased with increasing concentration and decreasing frequency. Usually the electrical crosstalk did not exceed 1% of the pickup signal, reaching in the most unfavorable case 5%. Only for $\alpha_{\text{expt}}>0.15$ cm^{-1}, the −3-dB points had to be corrected for the crosstalk to find the −3-dB points of the signal without crosstalk.

When investigating a cylinder harmonic with a frequency between 40 and 630 kHz, we use the temperature dependence of the sound velocity in the torus at $\omega/2\pi=9$ kHz as an independent reference, especially to determine T_λ^s. Vice versa the cylinder at 40 kHz is used for control, while investigating resonances at 2 kHz $\leq\omega/2\pi\leq$ 20 kHz in the torus. This allows a temperature scale independent of the germanium thermometer.

IV. EXPERIMENTAL RESULTS AND ANALYSIS OF THERMODYNAMIC VELOCITY

A. Influence of gravity

The λ transition is pressure sensitive with a slope $(\partial T/\partial P)_\lambda<0$. For a sample of finite height the gravity induced pressure gradient leads to a lower T_λ at the bottom than at the top of the cell.[42] For a 0.5-cm-high resonator the spread in transition temperature is 0.6 μK for ^{4}He. The absolute value of the slope $(\partial T/\partial P)_\lambda$ of the λ line increases with ^{3}He concentration, being about 15% larger at $X_3=0.15$ than at $X_3=0$.[46,47] No information is available at higher concentrations. For our mixtures with $X_3<0.2$ the spread in transition temperature is $\lesssim$0.8 μK, so that for these samples gravity effects are limited to a very narrow region around T_λ. For $X_3=0.517$ and $X_3=0.377$, the temperature dependence of attenuation and dispersion near T_λ is already much weaker than at lower X_3 (see Figs. 7 and 9). Therefore, even a somewhat larger spread of the transition temperature at these concentrations would have a negligible influence on our conclusions.

B. Sound velocity and related thermodynamic parameters

Our measurements of resonant frequencies of the helium-filled cavities are much more precise than any determination of the effective cavity length. To convert our frequencies to sound velocities, we normalized the ^{4}He data for $\omega/2\pi\leq$ 20 kHz to the value $u(0)=21\,800.0$ cm/sec at $T-T_\lambda^s=-40$ μK, where dispersion and gravity effects are negligible, and the velocity varies very mildly with temperature. This normalization at finite t and low frequency in a region without dispersion is likely to be more reliable and accurate than a least-squares fit of the data to $u(\omega\gtrsim 0)$ and then normalizing at T_λ. Our normalization value is consistent with that of previous work, $u_\lambda(0)=21\,730.0$ cm/sec.[8,10,12,17] In each run, data were taken at one of our reference frequencies, $\omega/2\pi=9$ or 40 kHz, and simultaneously at a second frequency. The data taken at this second frequency were normalized to the 9-kHz data at a temperature far enough below T_λ where no dispersion occurs. Hence, all our velocity data are normalized to $u(0)=21\,800$ cm/sec for ^{4}He at $T-T_\lambda^s=-40$ μK. Examples[49] are shown in Fig. 4 where the thermodynamic velocity $u(0)$ as well as the velocity $u(\omega)$ at various frequencies between 2.3 and 627 kHz are plotted for $X_3=0.070$, 0.377, and 0.517. The velocity scales have different resolution and are referenced to $u_\lambda(0)$, the value of the thermodynamic velocity at T_λ (see Table II).

The values for the velocity of sound for $\omega/2\pi=9$ and 20 kHz were fit to Eq. (1) over the temperature range 20 μK $\leq|T-T_\lambda^s|\leq$ 1 mK, a range which is clearly free of dispersion at these frequencies or gravity effects (see Fig. 4). These fits were performed independently for $T<T_\lambda$ and $T>T_\lambda$. For the specific heat we used the closed-form expression $C_p=(A/\alpha)(t^{-\alpha}-1)+B$ with coefficients given in Ref. 26. Because the peak of C_p near T_λ decreases with increasing X_3,[20] the minimum of u near T_λ becomes less distinct with increasing X_3 (see Fig. 4). The differences $u_{\text{measured}}-u_{\text{fit}}$ usually are less than 0.1 cm/sec for 20 μK $\leq|T-T_\lambda^s|\leq$ 1

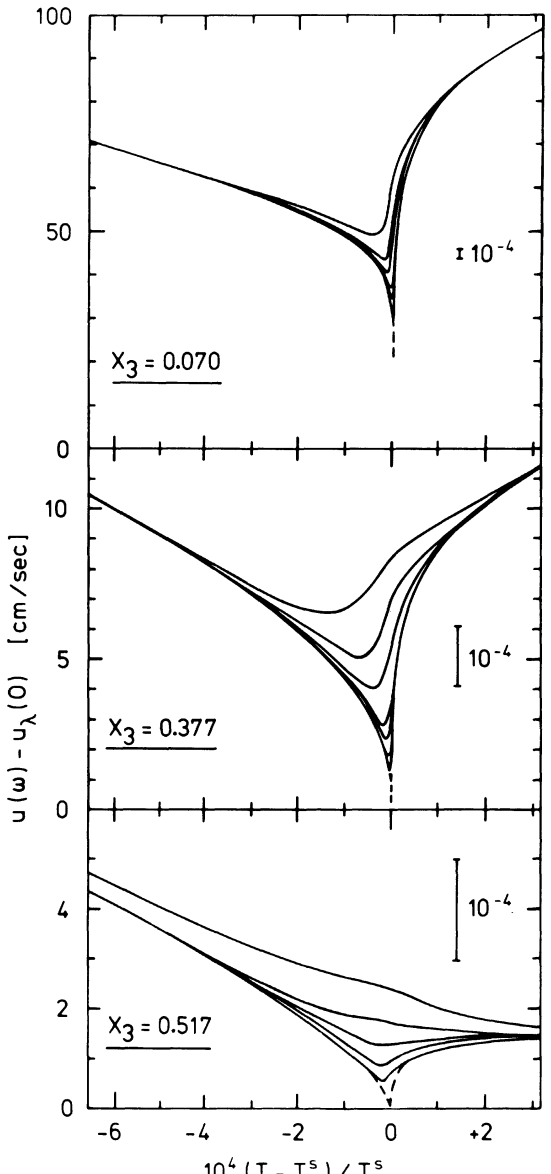

FIG. 4. Measured first sound velocity $u(\omega)$ minus $u_\lambda(0)$ as a function of $(T - T_\lambda^s)/T_\lambda^s$ for the three indicated mixtures (Ref. 49). $u_\lambda(0)$ is the zero-frequency velocity in a zero-height sample at T_λ obtained from a fit of Eq. (1) to our low-frequency data (see Table II). T_λ^s is the λ temperature at the top of our sample. The data are for $\omega/2\pi = 627.4$, 193.8, 107.7, 43.1, 20.6, and 9.16 kHz (indistinguishable on this scale from 4.6 and 2.3 kHz) for $X_3 = 0.070$; for $\omega/2\pi = 598.3$, 205.4, 102.7, 41.1, 21.8, 10.9, and 4.4 kHz (indistinguishable on this scale from 2.3 kHz) for $X_3 = 0.377$; and for $\omega/2\pi = 604.2$, 241.6, 100.6, 40.3, and 10.7 kHz at $X_3 = 0.517$. The dashed lines are the gravity-corrected thermodynamic velocities $u(\omega = 0, h = 0.5$ cm), calculated with Eq. (1) from a fit of our data at 9 and 20 kHz for $20\ \mu\text{K} \leq |T - T_\lambda^s| \leq 1$ mK, where no dispersion occurs. Note the increasing resolution of the velocity scale, necessary to show the weak dispersion at the higher ^{3}He concentrations.

mK and at all X_3.

The values of $u_\lambda(0)$ calculated from the data at $T < T_\lambda$ and at $T > T_\lambda$ agree to within 2 cm/sec for $X_3 < 0.2$, and to within 0.5 cm/sec for the higher concentrations. The values for $u_\lambda(0)$ are given in Table II. This table also contains $u_{\min}$ (2.3 kHz) $- u_\lambda(0)$, where $u_{\min}(2.3\ \text{kHz})$ is the minimum velocity measured at $\omega/2\pi = 2.3$ kHz; this difference decreases strongly with ^{3}He concentration. In addition, we give in Table II the values for the difference between the minimum thermodynamic velocity in an $h = 0.5$-cm-high sample and the thermodynamic velocity in a sample of zero height at T_λ, $u_{\min}(0) - u_\lambda(0)$. $u_{\min}(0)$ is obtained from the mentioned fit of Eq. (1) to our data using[46,47] $\rho g h(\partial T/\partial P)_\lambda = 0.6$, 0.6, 0.8, 1, and 2 μK for $X_3 = 0$, 0.07, 0.194, 0.377, and 0.517, respectively, for the calculation of the influence of gravity on $u(0)$ close to T_λ.[17] The values for the thermodynamic velocity very near to T_λ depend on the detailed behavior of C_p. We attribute the difference between the value for $u_{\min}(0) - u_\lambda(0)$ at $X_3 = 0$ obtained here, and the value of Ref. 17 to the different equations used for the t dependence of C_p.[26] For the thermodynamic velocity at T_λ we find the following concentration dependence:

$$u_\lambda(0) = 21\,736 - 3182 X_3 + 173 X_3^2$$

to within $\Delta u/u \simeq 10^{-4}$.

From the values for the coefficient a of Eq. (1), which is related to thermodynamic quantities, we calculated $(\partial S/\partial P)_\lambda$, using published data for V_λ,[48] and our data for T_λ and $u_\lambda(0)$ (see Tables I and II). The values obtained from data at $T < T_\lambda$ and at $T > T_\lambda$ are shown as a function of X_3 in Fig. 5. The two values at each X_3 generally agree within their errors, and they agree well with earlier published values.[12,13,17] The systematic difference $(\partial S/\partial P)_\lambda^+ > (\partial S/\partial P)_\lambda^-$ is attributed to the uncertainties in the coefficients A, α, and B of the specific heat,[26] and to the fact that the asymptotic values for $(\partial S/\partial P)_\lambda$ are determined from a fit of data measured at finite t. The values for $(\partial S/\partial P)_\lambda$ increase with ^{3}He concentration by less than a factor of 2 in our concentration range.

With the relation[17]

$$\left(\frac{\partial V}{\partial P}\right)_\lambda = -\left(\frac{V_\lambda}{u_\lambda}\right)^2 + \left(\frac{\partial T}{\partial P}\right)_\lambda \left(\frac{\partial S}{\partial P}\right)_\lambda - \frac{T}{C_p}\left(\frac{\partial S}{\partial P}\right)_\lambda^2 , \tag{10}$$

where all quantities are per unit mass, we calculated $(\partial V/\partial P)_\lambda$ for the mixtures. We used V_λ of Ref. 48, C_p from Ref. 26, and our data for u_λ and $(\partial S/\partial P)_\lambda$. For $(\partial T/\partial P)_\lambda$ we used the values for $X_3 \leq 0.15$ of Refs. 46 and 47, and extrapolated them for higher concentrations to the above given values.

TABLE II. Thermodynamic velocity and related parameters.

X_3	0	0.070	0.194	0.377	0.517
$u_\lambda(0)$ (cm/sec) [a]	21 734.0	21 517.7	21 126.0	20 559.2	20 138.9
$u_{min}(0) - u_\lambda(0)$ (cm/sec) [b]	39.7	21.2	7.6	0.4	0.1
$u_{min}(2.3\text{ kHz}) - u_\lambda(0)$ (cm/sec) [c]	52.6	29.1	10.8	1.3	0.5 [d]
$u(600\text{ kHz}, T_\lambda) - u_\lambda(0)$ (cm/sec) [e]	95.0	63.3	33.7	8.4	2.4
$\left(\frac{\partial S}{\partial P}\right)_\lambda \left(\frac{\text{cm}^3}{\text{mole K}}\right)$	−0.968	−0.921	−0.890	−0.724	−0.615
$10^7\left(\frac{\partial V}{\partial P}\right)_\lambda \left(\frac{\text{cm}^5}{\text{mole dyne}}\right)$	−3.89	−4.23	−4.91	−6.06	−7.13

[a] Normalized at $u(0) \equiv 21\,800.0$ cm/sec for ^{4}He at $T - T_\lambda^s = -40$ μK.

[b] $u_{min}(0)$ is the minimum thermodynamic velocity for a 0.5-cm-high sample obtained from a fit of Eq. (1) to our data at 9 and 20 kHz for $20\ \mu\text{K} \leq |T_\lambda^s - T| \leq 1$ mK.

[c] $u_{min}(2.3\text{ kHz})$ is the minimum velocity measured at 2.3 kHz.

[d] $u_{min}(10.7\text{ kHz}) - u_\lambda(0)$.

[e] $u(600\text{ kHz}, T_\lambda)$ is a measured velocity, which is not noticeably influenced by gravity (Ref. 15).

Since the second term of Eq. (10) contributes less than 1% to $(\partial V/\partial P)_\lambda$, this extrapolation is a sufficient approximation. The values obtained for $(\partial V/\partial P)_\lambda$ are given in Table II.

C. Dispersion of sound

At finite ω the dip in u near T_λ becomes less distinct due to dispersion of sound.[10] Figure 4 demonstrates the drastic decrease of the dispersion with increasing ^{3}He concentration. In addition, the dispersion extends to larger t for increasing X_3. At $X_3 = 0.517$ and $\omega/2\pi \geq 200$ kHz, the dispersion more than compensates the C_p^{-1} dip of the thermodynamic velocity, so that no minimum in $u(\omega)$ can be resolved. One may also see how the minimum in u, which for $\omega = 0$ occurs at $T_\lambda^{\text{bottom}}$,[17] moves away from T_λ with increasing ω.

From the velocity data we determined $u(\omega/2\pi) - u(2.3\text{ kHz})$, as well as the sound dispersion $D = u(\omega) - u(0)$. As examples[49] we show in Fig. 6 these two differences for $X_3 = 0.377$ at all investigated frequencies (cf. to $X_3 = 0.194$ in Ref. 16), and

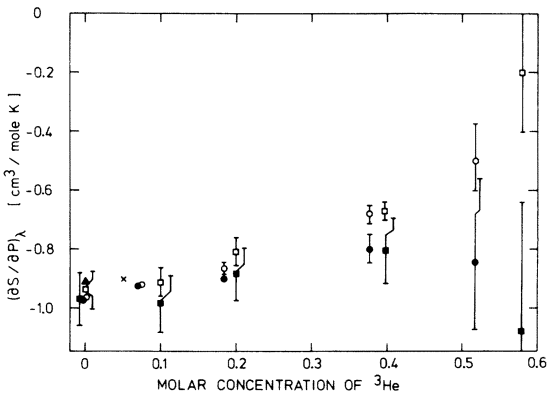

FIG. 5. $(\partial S/\partial P)_\lambda$ vs molar ^{3}He concentration. The shown values are from fits of Eq. (1) to data measured at $T < T_\lambda$(●), and at $T > T_\lambda$(○). The corresponding squares are from Ref. 13, the cross is from Ref. 12, and the triangle is from Ref. 17. The error bars on the present data are shown only if greater than the data points. They correspond to an uncertainty of 0.3 cm/sec for the sound velocity, and the resulting deviation for the fitted parameter "a" in Eq. (1). Errors resulting from the unknown uncertainties in the used parameters for the specific heat (Ref. 26) are not included.

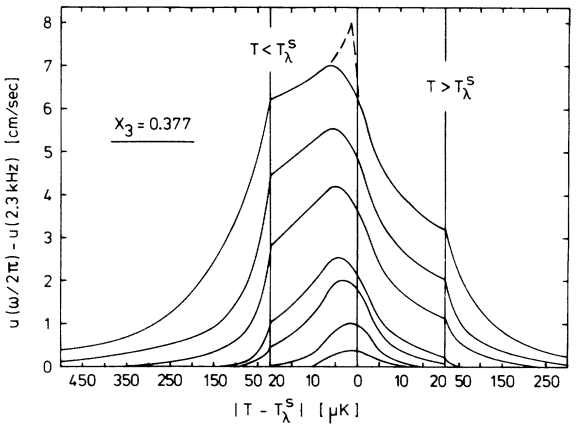

FIG. 6. Measured velocity difference $u(\omega/2\pi) - u(2.3\text{ kHz})$ for $X_3 = 0.377$ as a function of $|T - T_\lambda^s|$. The data are for $\omega/2\pi = 598.3$, 205.4, 102.7, 41.1, 21.8, 10.9, and 4.4 kHz, in decreasing order. The dispersion $u(2.3\text{ kHz}) - u(0)$, which has to be added to each of the shown curves to obtain the dispersion $u(\omega) - u(0)$, is the dashed peak on top of the highest-frequency curve. $u(0)$ is the thermodynamic velocity of sound in a 0.5-cm-high sample. Note the changes in temperature scale at $|T - T_\lambda^s| = 20$ μK.

in Fig. 7 we show D for $\omega/2\pi \simeq 600$ kHz at all investigated mixtures. Qualitatively the results at each frequency and mixture show the same behavior as a function of temperature. The measured dispersion is asymmetric around T_λ^s with a peak on the low-temperature side. It is appreciably smaller at $T > T_\lambda^s$ than at $T < T_\lambda^s$. The dispersion $u(\omega) - u(0)$ in the mixtures becomes clearly smaller than in pure ^{4}He at the same frequency; in Table II we give the value for $u(600\text{ kHz}, T_\lambda) - u_\lambda(0)$. Another influence of increasing X_3 is the slower decrease of the dispersion with increasing $t = |T - T_\lambda^s|/T_\lambda^s$. The maximum of the dispersion occurs slightly below T_λ^s because we have a sample of finite height, and refer all temperatures to the temperature T_λ^s when the transition occurs at the top of our sample. Figure 6 demonstrates that even at $\omega/2\pi = 2.3$ kHz there is appreciable dispersion at $|T_\lambda^s - T| < 5$ μK. The dispersion $u(2.3\text{ kHz}) - u(0)$ (the dashed dip in Fig. 6) is strongly influenced by the detailed behavior of $u(0)$, and therefore of C_p. Because of this strong dependence on C_p, whose investigation is not an object of this paper, we decided to analyze the dispersion in a region only where $u(2.3\text{ kHz}) - u(0) = 0$; we choose $|T - T_\lambda^s| > 5$ μK for the analysis. The frequency of 2.3 kHz is so low, and the height of our samples is so small that $u(\omega/2\pi) - u(2.3\text{ kHz})$ represents the dispersion $u(\omega) - u(0)$ for a sample of zero height except for -5 μK $\lesssim T - T_\lambda^s \lesssim 1$ μK which we exclude from the analysis.

D. Attenuation of sound

Examples[49] for the temperature dependence of the attenuation α for $X_3 = 0.194$ at various frequencies, and at $\omega/2\pi \simeq 600$ kHz for all investigated mixtures are shown in Figs. 8 and 9, respectively. The shape of α as a function of temperature is qualitatively the same at all ω and X_3. The attenuation α, too, is asymmetric about T_λ^s with a peak in the superfluid phase. It is a smooth, nonsingular function of t. Its strength is strongly reduced with increasing ^{3}He concentration, as expected from the behavior of the dispersion. At the same time the maximum of α moves away from T_λ with increasing ω or X_3, and the attenuation seems to extend over a broader t range with increasing X_3. The concentration dependence of the maximum of the attenuation, and of the attenuation near T_λ^s are shown in Fig. 10. They both decrease by roughly

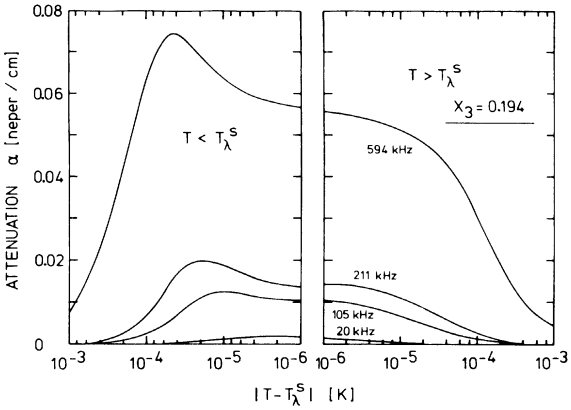

FIG. 8. Attenuation α for $X_3 = 0.194$ and at the indicated sound frequencies as a function of $|T - T_\lambda^s|$. A temperature independent background has been subtracted from the measured data in order to study the attenuation associated with the λ transition only.

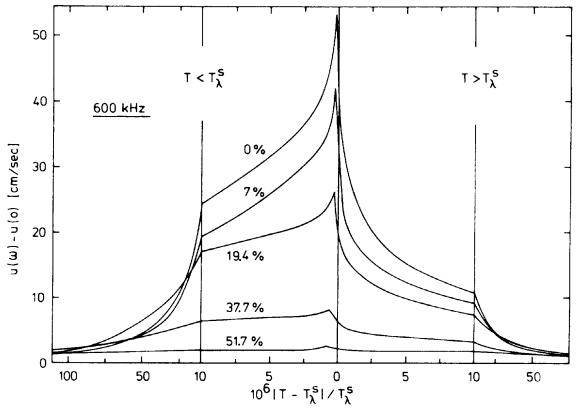

FIG. 7. Dispersion $u(600\text{ kHz}) - u(0)$ for ^{3}He–^{4}He mixtures with the indicated molar ^{3}He concentrations as a function of $|T - T_\lambda^s|/T_\lambda^s$ at a frequency of about 600 kHz. The exact frequencies used in the individual runs are given in Ref. 15. Note the changes in temperature scale at $|T - T_\lambda^s|/T_\lambda^s = 10^{-5}$.

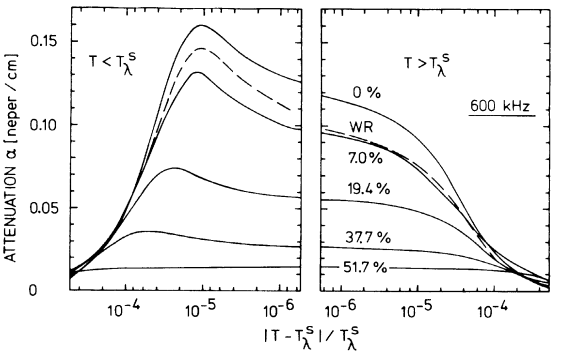

FIG. 9. Attenuation α for mixtures with the indicated molar ^{3}He concentrations as a function of $|T - T_\lambda^s|/T^s$ at a frequency of about 600 kHz. The exact frequencies are given in Ref. 15. A temperature-independent background has been subtracted from the measured data in order to study the attenuation associated with the λ transition only. The dashed line is the result of Williams and Rudnick for $X_3 = 0$ and $\omega/2\pi = 600$ kHz (Ref. 9).

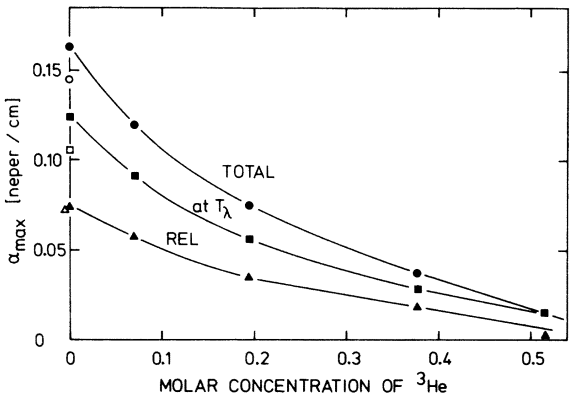

FIG. 10. Values of the maximum of the total attenuation (●), of the attenuation near T_λ (■), and of the maximum of the relaxation attenuation (▲) at $\omega/2\pi \simeq 600$ kHz (Ref. 15) as a function of ^{3}He concentration. The full lines are a guide for the eye only. The open symbols are the corresponding results of Ref. 9 for ^{4}He and 600 kHz.

one order of magnitude if X_3 is increased from 0 to 0.517. Because the temperature dependence of the attenuation near T_λ is very weak (see Figs. 8 and 9), we used data for $|T - T_\lambda^s| > 1$ μK for the analysis of the attenuation.

E. Comparison to other author's results

The value of α observed by Barmatz and Rudnick[8] for ^{4}He at 22 kHz is roughly a factor of 2 larger than our data. We disagree with their observation that $\alpha^+ > \alpha^-$. The t dependence and the absolute magnitude of our data for ^{4}He are in very good agreement with the results of Ref. 9 for $X_3 = 0$ at 600 kHz. This is demonstrated in Fig. 9 where it can be seen that the two sets of data agree to within 10% for $T < T_\lambda$, and to within (15–20)% for $T > T_\lambda$. Because two quite different methods have been applied to measure α in Ref. 9 and in this work, we consider the agreement in absolute magnitude to within the given limits as very satisfying. The frequency dependence of the maximum of the attenuation of our data, taken at $\omega/2\pi \leq 600$ kHz, scales very well with the results of Williams and Rudnick at 600 kHz $\leq \omega/2\pi \leq 3.17$ MHz (see below).

Our observation of a decrease of the dip in u and of the peak in α with increasing X_3 is in agreement with the qualitative observation of these phenomena by Roberts and Sydoriak at $\omega/2\pi = 5$ MHz.[11] Dyumin *et al.*[50] have measured α at 9.56 MHz and for $t > 2\times10^{-3}$ in mixtures with $X_3 = 0$, 0.063, 0.110, 0.197, and 0.314. Their data have less resolution in α and t. For $5\times10^{-2} \leq t \leq 2\times10^{-3}$ they find an attenuation of roughly 0.3 cm^{-1}, which seems to be essentially concentration independent.

A detailed comparison of our dispersion data to former results[7,8,10] does not seem to be appropriate because those results are appreciably influenced by gravity (which can be very severe for dispersion measurements if the sample height is not small enough), and insufficient temperature homogeneity at $T > T_\lambda$.

V. ANALYSIS AND INTERPRETATION OF DATA FOR DISPERSION AND ATTENUATION OF SOUND

A. Separation into relaxation and fluctuation contributions

1. Basis for separation (Ref. 51)

There is experimental[9,10] and theoretical[23,34] evidence that for our frequency range attenuation and dispersion of sound near T_λ are arising from order-parameter relaxation below T_λ and order-parameter fluctuations on both sides of T_λ; the processes are assumed to be additive.[34] These ideas are the basis of the following discussion. We have then

$$\alpha^+ = \alpha_F^+, \quad \alpha^- = \alpha_F^- + \alpha_R, \tag{11}$$

and correspondingly for dispersion. We use: $\alpha^+ = \alpha(T > T_\lambda)$; $\alpha^- = \alpha(T < T_\lambda)$; α_F: absorption due to fluctuations only; α_R: absorption due to relaxation only; α: total measured absorption (minus temperature-independent background attenuation). The relaxation contribution is described by Eqs. (2)–(6). The fluctuation contribution, on the other hand, is known neither for ^{4}He nor for the mixtures in a functional form to which data could be compared in detail.[23,34] But it is expected that the fluctuation contributions above and below T_λ are about equal,[23] as supported by experimental results.[9,10] According to scaling,[3] α_F^+ and α_F^- should have the same t dependence. And, according to the universality concept, the ratio α_F^-/α_F^+ of the fluctuation contributions above and below T_λ on an appropriate temperature scale is expected to be independent of "the inert variable" concentration.[4,14] These predictions are inherent in the scaling form Eq. (7). In this analysis we used the following two approaches to take the fluctuation contribution to α and D into account, and to separate out the relaxation part:

(i) The functional dependences of α_F (and D_F) on *temperature* are the same above and below T_λ, but they may have different amplitudes in the superfluid and normal-fluid phases, respectively,

$$\alpha_F^-(t) = r\alpha_F^+(t), \tag{12}$$

with a factor r of order unity. This gives

$$\alpha_R = \alpha^- - \alpha_F^- = \alpha^- - r\alpha^+. \tag{13}$$

A shortcoming of this approach is the fact that factors $r \neq 1$ introduce discontinuities in α (or D) at T_λ (in contradiction to our experimental results).

(ii) A characteristic time or a correlation length might be the more appropriate scale than temperature for critical phenomena. In a second approach, therefore, we assume that the functional dependence of α_F (and D_F) on the *characteristic time* τ is the same above and below the transition,

$$\alpha_F^-(\tau^-) = \alpha_F^+(\tau^+) \quad \text{at } \tau^- = \tau^+ . \tag{14}$$

According to scaling

$$\tau^- = \tau_0^- t^{-x^-}; \quad \tau^+ = \tau_0^+ t^{-x^+}, \tag{15}$$

with $x^- = x^+ = x$, but possibly $\tau_0^- \neq \tau_0^+$. Hence, we assume

$$\alpha_F^-(t) = \alpha_F^+(qt) \tag{16}$$

and get

$$\alpha_R(t) = \alpha^-(t) - \alpha_F^-(t) = \alpha^-(t) - \alpha^+(qt) . \tag{17}$$

The factor $q = (\tau_0^-/\tau_0^+)^{1/x}$ should be of order unity.[14,29]

The relaxation contribution α_R (and D_R, respectively) was obtained by subtracting the data measured above T_λ from those measured below T_λ, according to Eqs. (13) or (17). The obtained α_R (and D_R) were fit to Eq. (6) with the values for $3\nu' - 2$ from Table I and parameters for C_p from Ref. 26. In these nonlinear least-squares fits we first used A_R, τ_0', x', and q (or r) as fit parameters. We obtained optimum values for the exponent x', which were scattering around $x' = \nu' + w$, with ν' and w determined in independent measurements of ξ' and u_2 (see Table I).[26,31] This scatter induces a very broad scattering of τ_0', because of the strong correlation between x' and τ_0'. We then fixed x' to the value $\nu' + w$ [see Eq. (2)]. With these fixed values for x', absorption data for $|T - T_\lambda^s| \geq 1$ μK, and dispersion data for $|T - T_\lambda^s| \geq 5$ μK were fit independently for each mixture and each frequency. For ease of computation, r (or q) was fixed, and A_R and τ_0' fit as usual. Then r (or q) was changed by a step, the whole procedure repeated, and after sufficient steps, finally, the absolute minimum of the sum of squares of deviations determined the optimum values for r (or q), A_R, and τ_0'.

2. *Results of this analysis*

The attenuation and dispersion remaining after the subtraction procedure [Eqs. (13) and (17)] could be fit rather well to Eq. (6). Varying the amplitude factor r between 0.8 and 1.2, or the factor q for the temperature scale between 0 and 2.5, and looking for the best fit resulted in a broad, insignificant scatter of r and q around the value 1, without systematic deviations or appreciable influence on the fit parameters.[52] Often the best fit actually was obtained for $r = q = 1$, or very close to this value. We conclude that our data for the attenuation and dispersion for the investigated mixtures and frequencies do indicate that the fluctuation contribution to α and D is very similar in the superfluid and normalfluid phase if Eqs. (2)–(6) and Eqs. (13) or (17) are correct. In the following, we discuss the results for $r = q = 1$, which are representative for all fits with r and q varied within the mentioned ranges.

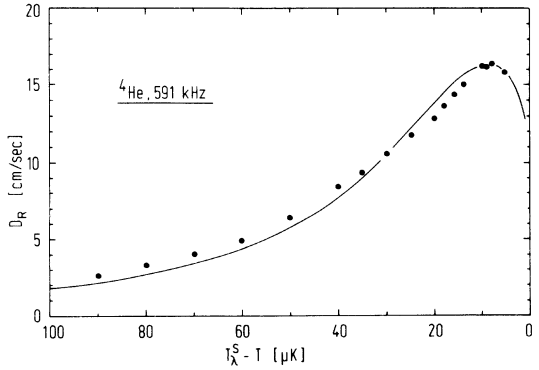

FIG. 11. Relaxation part D_R of the dispersion as a function of $T_\lambda^s - T$ for ^{4}He and $\omega/2\pi = 591$ kHz. The few data points represent a continuous measurement and are the difference between the dispersion measured below and above T_λ^s, at $|T - T_\lambda^s| \geq 5$ μK. The full line is a fit of Eq. (6) with $x' = 1.062$, and A_R and τ_0' as free parameters to the shown data.

Examples for the fits of α_R and D_R are shown in Figs. 11 and 12 for ^{4}He at 591 kHz.[49] The attenuation α_R is a nearly symmetric function of $\log_{10}(t)$, as expected from Eq. (2) (see also Fig. 15). The agreement between the fitted curves and data for

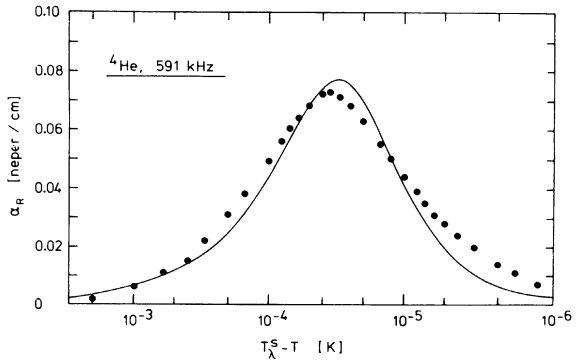

FIG. 12. Relaxation part α_R of the attenuation as a function of $T_\lambda^s - T$ for ^{4}He and $\omega/2\pi = 591$ kHz. The few data points represent a continuous measurement and are the difference $\alpha^- - \alpha^+$ of the attenuation measured below and above T_λ^s. The full line is the fit of Eq. (6) with $x' = 1.062$, and A_R and τ_0' as free parameters to the shown data.

α_R and D_R is within the precision of our data. But, we observe a small systematic deviation because the data for α_R, e.g., show a slightly larger half-width than the fitted curves, if plotted on a logarithmic temperature scale (cf. Fig. 12). It is not possible to overcome this problem with differently chosen parameters. We reanalyzed the data of Ref. 9 with the correct Eqs. (2) to (6), and observed exactly the same effect.[53]

In Fig. 10 we show the decrease of the maximum relaxation attenuation $\alpha_{R,\max}$ with increasing ^{3}He concentration, as well as the maximum total attenuation, and the maximum fluctuation attenuation $\alpha(T \simeq T_\lambda)$. These results demonstrate the similar behavior of the strength of the relaxation and the fluctuation attenuation, which agree to within a factor of about 2, at least for $X_3 < 0.4$. The dispersion, $u(600\ \text{kHz}, T_\lambda) - u_\lambda(0)$, shows a somewhat stronger decrease with increasing concentration X_3. The consistency between our dispersion and absorption data is confirmed by the agreement of the parameters A_R and τ_0', obtained from independent fits of α_R and D_R. The results for A_R and τ_0', as a function of X_3, are shown in Figs. 13 and 14, and in Table III.[54] The amplitude A_R decreases by almost three orders of magnitude when X_3 is increased from 0 to 0.517. The $\log_{10} A_R$ seems to decrease linearly with X_3. The corresponding decrease of Δu with concentration is strongly reduced by the factor $t^{3\nu'-2} C_p^{-2}$ [see Eq. (4)]. In addition, we show in Fig. 13 the values for A_R calculated from Eq. (5). For this calculation we used T_λ and ξ from Table I, our values for u_λ and $(\partial S/\partial P)_\lambda$ from Table II, $\xi_0' = \tau_0' u_{20}$ with τ_0' from our data (Table III), V_λ from Ref. 48, and u_{20} and ρ_s from Ref. 26. There is no adjustable parameter, and the two curves in Fig. 13 are *not* normalized at $X_3 = 0$. The very good agreement in absolute magnitude and in concentration dependence is a strong support for our analysis. The fitted values of A_R depend on the exponent $3\nu' - 2$ and on the specific heat C_p [Eq. (6)]; the deviation from the measured values for the higher X_3 may result from uncertainties in $3\nu' - 2$ or in C_p for these concentrations.[20,26,31,32]

The amplitude τ_0' of the relaxation time increases by more than one order of magnitude in the investigated concentration range (see Fig. 14). The increase of $\log_{10} \tau_0'$, again, occurs approximately linear with X_3 for $X_3 < 0.4$. Our value $\tau_0' = (2.01 \pm 0.3) \times 10^{-12}$ sec at $X_3 = 0$ corresponds to $\xi_0' = \tau_0' / u_{2,0} = (0.93 \pm 0.14)$ Å, which is in quite good agreement with experimental results of others.[9,30,37] In addition, we have plotted in Fig. 14 the value $\tau_0' = 1.45 \times 10^{-12}$ sec, which we obtained from a fit of William's and Rudnick's data for ^{4}He at $\omega/2\pi = 600$ kHz to 3.17 MHz.[9,53] We also show τ_0 from a

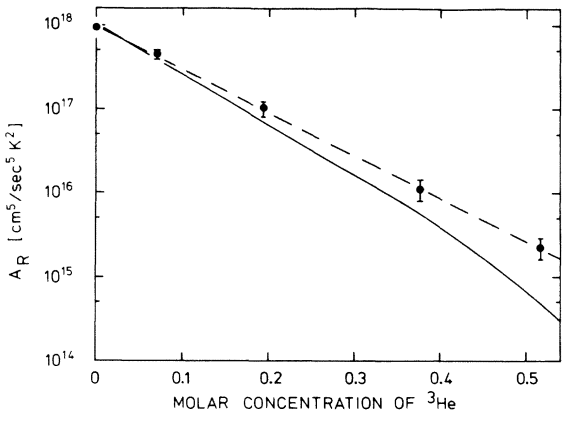

FIG. 13. Amplitude A_R of $\Delta u = u(\infty) - u(0)$ [see Eq. (4)] as a function of ^{3}He concentration. The points are the mean values determined from a fit of Eq. (6) to the relaxation part of the attenuation and dispersion at various frequencies (Ref. 54). The data obtained from α_R and D_R agree within their errors. Note the drastic decrease of A_R with X_3. The dashed straight line through the data is a guide for the eye only. The value of Ref. 9 for $X_3 = 0$ coincides with our result, if their data are reanalysed with Eq. (6) (Ref. 53). The full line is calculated with no adjusted parameter from Eq. (5) (Ref. 25); the curves are *not* normalized at $X_3 = 0$.

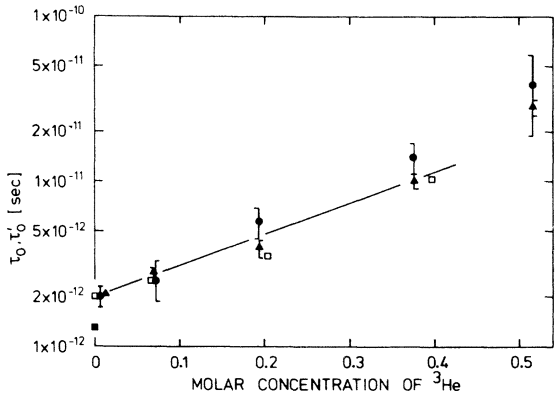

FIG. 14. Amplitude τ_0' of the relaxation time $\tau' = \tau_0' t^{-x'}$ as a function of ^{3}He concentration. The full dots (●) are the mean values from fits of Eq. (6) with x' from Table I to the relaxation part of the attenuation and dispersion at various frequencies (Ref. 54). The data obtained from α_R and D_R agree within their errors. The triangles (▲) are the values for τ_0 obtained from the scaling analysis of α and D at $T > T_\lambda$ described in Sec. V D; they are normalized to $\tau_0' = 2.01 \times 10^{-12}$ sec for $X_3 = 0$. At the same value the data (□) are normalized for $\tau_0' = \xi_0' / u_{2,0}$ obtained from measurements of correlation length ξ', and velocity u_2 of second sound as reported in Ref. 31. If the data of Ref. 9 are analysed as described in the text, they give the full square (■) for $X_3 = 0$ (Ref. 53). The straight line is a guide for the eye only.

TABLE III. Results from analysis of dispersion and attenuation (Ref. 54).

X_3	0	0.070	0.194	0.377	0.517
$10^{-15}A_R$ ($cm^5/K^2\,sec^5$)	925 ±75	445 ±52	102 ±21	11.1 ±3.1	2.33 ±0.53
$10^{12}\tau_0'$ (sec) [a]	2.01 ±0.3	2.56 ±0.7	5.68 ±1.2	14.1 ±2.9	39 ±20
$10^{12}\tau_0$ (sec) [b]	(2.01)	2.79 ±0.2	4.02 ±0.5	10.1 ±1.0	29 ±3
ξ_0' (Å) [c]	0.93	1.21	2.49	4.57	8.8

[a] From analysis of the relaxation contribution (Sec. V A).
[b] From scaling analysis with $x = x' = \nu' + w$, and normalized to $\tau_0'(0) = 2.01 \times 10^{12}$ sec (Sec. V D).
[c] From $\xi_0' = u_{2,0}\,\tau_0'$, with $u_{2,0}$ from Ref. 26.

scaling analysis of our data at $T > T_\lambda$, to be discussed below (see Table III), and values which we obtain from $\tau_0' = \xi_0'/u_{2,0}$, using published values for the healing length and the velocity of second sound of the mixtures.[26,31] The obtained agreement gives us confidence in the discussed analysis. Our results disagree with $\tau' = 0.65 \times 10^{-12} t^{-1.45\pm0.1}$ sec reported recently in Ref. 35 for $X_3 = 0.36$ and $\omega/2\pi = 36$ MHz.

3. *Temperature dependence of position of maximum of relaxation attenuation*

The maximum $\alpha_{R,\max}$ of the relaxation attenuation at constant ω moves away from T_λ with increasing X_3, since the amplitude τ_0' of the relaxation time increases with X_3. This is shown in Fig. 15 for $\omega/2\pi \simeq 600$ kHz.

We only have $\omega\tau' = 1$ at $\alpha_{R,\max}$ if the temperature dependence of Δu is neglected. With Eq. (6) we find for the maximum $\alpha_{R,\max}$ of the relaxation attenuation

$$(\omega\tau')^2 = \frac{x' - (3\nu' - 2) - 2\alpha'\varphi(t)}{x' + (3\nu' - 2) + 2\alpha'\varphi(t)} \leq 1 \quad \text{at } \alpha_{R,\max},$$

with

$$\varphi(t) = [1 - t^{\alpha'}(1 - \alpha' B'/A')]^{-1},$$

and parameters from the specific heat $C_p = (A'/\alpha')(t^{-\alpha'} - 1) + B'$. The value of $\omega\tau'$ at $\alpha_{R,\max}$ changes by less than 3% per decade of t in our temperature range, and is essentially determined by the exponents x', ν', and α'. Its values, calculated at $t = 10^{-5}$, are given in Table I.

Neglecting the weak t dependence of $\omega\tau'$ at $\alpha_{R,\max}$ (i.e., $\omega\tau' = \text{const}$ at $\alpha_{R,\max}$), and plotting $t_{R,\max}$ (the reduced temperature difference at $\alpha_{R,\max}$) versus frequency, we can determine the critical exponent x' of τ' [see Eq. (2)], which is the slope in a log-log plot. An example of such a plot is shown for $X_3 = 0.194$ in Fig. 16. A least-squares fit of $\tau' = \tau_0' t^{-x'}$ yields

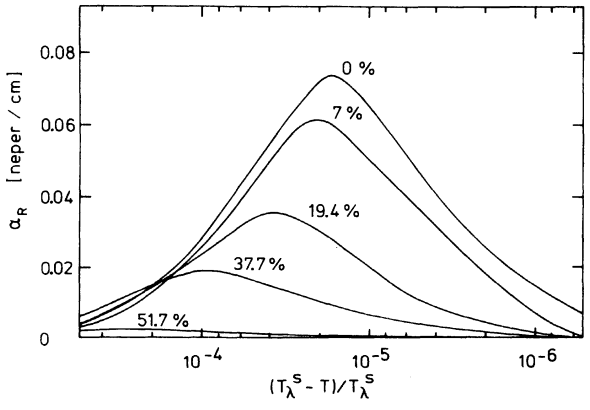

FIG. 15. Relaxation part $\alpha_R = \alpha^- - \alpha^+$ of the attenuation, obtained by subtracting the attenuation measured above T_λ^s from the attenuation measured below T_λ^s, as a function of $(T_\lambda^s - T)/T_\lambda^s$ for the indicated mixtures at $\omega/2\pi \simeq 600$ kHz (Ref. 15).

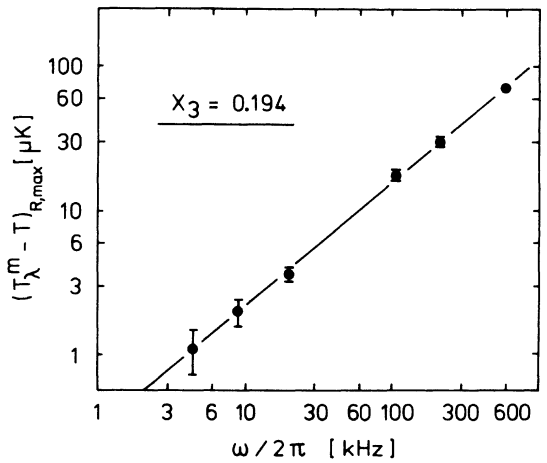

FIG. 16. Temperature difference $(T_\lambda^m - T)_{R,\max}$ where the maximum of the relaxation attenuation occurs as a function of sound frequency for $X_3 = 0.194$. T_λ^m is the temperature when the λ transition reaches the middle of our 0.5-cm-high sample. The straight line corresponds to $\omega t^{-1.16} = \text{const}$. The slope represents the exponent and depends strongly on the value of T_λ^m due to the small values of $(T^m - T)_{R,\max}$ at low frequencies.

x' values for the investigated mixtures which are 0.1–0.2 higher than the values $x' = \nu' + w$. Taking the weak t dependence of $\omega\tau'$ at $\alpha_{R,\max}$ into account changes x' by less than 1%. Because of the rather small values of $t_{R,\max}$ at the low-frequency end of our range, changes of only a few 10^{-7} K in T_λ significantly influence the results for x'. For this analysis we used T_λ^m, the temperature of the λ transition at the middle of our 0.5-cm-high sample. Changing these values for T_λ^m by 0.5 μK gives values for x' from this analysis which agree with $x' = \nu' + w$. Such a shift in T_λ is within our uncertainty in determining the transition temperature; we therefore do not consider the above mentioned discrepancy for the values of x' to be significant, and still consider $x' = \nu' + w$ to be valid.

The maximum of the relaxation attenuation can occur significantly further away from T_λ than the maximum of the total attenuation; this fact has sometimes been neglected.[9,55]

B. Frequency dependences of α and D

Besides the temperature and concentration dependence, the frequency dependence of the attenuation and dispersion near T_λ is of particular importance. If we write for the maximum total attenuation, the maximum of its relaxation part, or the attenuation near T_λ (maximum fluctuation part),

$$\alpha = \alpha_0 \omega^{1+y}, \tag{18}$$

we find the exponents y given in Fig. 17.[56] The first remarkable result is the fact that for each of these three attenuation values the exponent y is the same (within our errors), except at $X_3 = 0.517$. Next we notice that y is about constant at 0.10 for $X_3 < 0.2$ and increases to about 0.4 for $X_3 = 0.517$ (except for the exponent of $\alpha_{R,\max}$). An exponent y larger than 0 is in agreement with the result $y = 0.15$ of Ref. 9 at 16 kHz $\leq \omega/2\pi \leq$ 3.17 MHz for ^{4}He, and $y = 0.17 \pm 0.1$ for $X_3 = 0.36$ and 1 MHz $\leq \omega/2\pi \leq$ 36 MHz given in Ref. 35. For higher frequencies, 0.6 MHz $\leq \omega/2\pi \leq$ 1 GHz, values for the exponent y of the attenuation at T_λ of about 0.3 have been reported for ^{4}He.[35,36,39]

The calculated amplitudes α_0 depend very strongly on the exponents y. We therefore hesitate to give absolute values, and remark only that α_0 decreases roughly from about 5×10^{-9} cm^{-1} to about 1×10^{-12} cm^{-1} for $X_3 = 0$ to $X_3 = 0.517$, within an uncertainty of about a factor of 2, and for our exponents y. For a better comparison of amplitudes use Fig. 10.

From the proportionality

$$u(\omega) - u_\lambda(0) \sim \omega^y \tag{19}$$

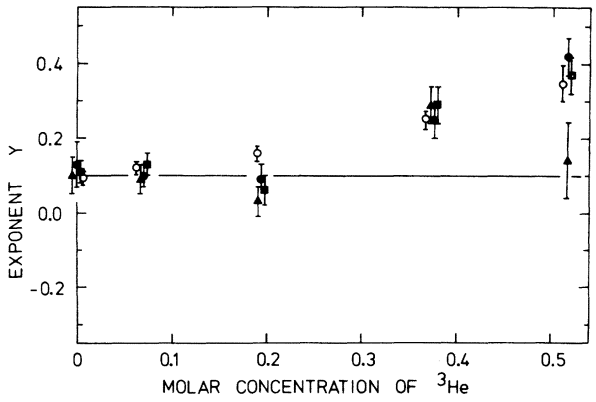

FIG. 17. Exponents of the frequency dependence of $\alpha = \alpha_0 \omega^{1+y}$ for the maximum of the total attenuation (■), for the maximum of the relaxation attenuation (▲), and for the attenuation near T_λ^s (●), respectively. The open circles (○) are the frequency exponents of the maximum dispersion $u(\omega) - u_\lambda(0) \sim \omega^y$. The investigated frequency range is 2.3 kHz $\leq \omega/2\pi \leq$ 627 kHz. The value of Ref. 9 for α at $X_3 = 0$ and 0.6 MHz $\leq \omega/2\pi \leq$ 3.17 MHz is $y = 0.15$, in good agreement with our results. The line at $y = 0.10$ is a guide for the eye only.

we find the frequency exponents y of the maximum dispersion which are also given in Fig. 17. The obtained values are in very good agreement with the corresponding values for the attenuation. But since y is small, we cannot distinguish between Eq. (19) and $u(\omega) - u_\lambda(0) \sim \log_{10}(\omega\tau)$, which is equally compatible with our data. The frequency dependences of the attenuation and dispersion described by the results given in Fig. 17 are in agreement with the prediction of Eq. (8) that $\alpha_F \sim \omega^{1+s/x}$ for constant $\omega\tau$, and $s > 0$.

C. Hydrodynamic regime

To check the compatibility of our data with the prediction of Eqs. (9) for the hydrodynamic regime, we plotted α/ω^2 and D/ω^2 vs $|T - T_\lambda|$. We find that our data fall onto one common curve, and allow Eqs. (9) only for $\omega\tau < 0.1$ on both sides of T_λ. Unfortunately, in this range α and D become rather small, and conclusions are subject to considerable uncertainties.

D. Scaling of dispersion and attenuation

Our attenuation and dispersion data at all ω and X_3 behave qualitatively similar. Hence, one may expect that by using an appropriate scaling variable the results for all ω and X_3 may collapse onto a single curve, and one may be able to determine the form of the scaling function. Therefore, a more general analysis of our data based on scaling assumptions was performed by fitting them to

scaling equations like Eq. (8) with the variable $\omega\tau$. Recently, this approach has been applied also by Golding[55] to sound attenuation at the ferromagnetic transition of MnP, and by Ref. 35 in a preliminary analysis of sound attenuation near the λ transition of ^{4}He and of a ^{3}He-^{4}He mixture ($X_3 = 0.36$) for frequencies from 1 to 15 MHz.

1. Attenuation at $T > T_\lambda$

Data below and above T_λ are treated separately, and the exponent and amplitude of the characteristic time $\tau = \tau_0 t^{-x}$ are determined independently.

All data are normalized to their values near T_λ, which means at large $\omega\tau$. This normalization removes the frequency factor ω^{1+y} from α, leaving $\alpha_F \sim f_F(\omega\tau)$ only; a normalization at $\omega\tau = 1$ gives the same results.[56] The data for each mixture have been plotted as a function of ωt^{-x} for various x in the range $0.9 \leq x \leq 1.4$. These plots show that the best agreement of the data measured at various ω is obtained for $x = 1.10 \pm 0.05$ for all investigated mixtures. Actually, within the given resolution we cannot distinguish whether the best matching of the data to one curve for each mixture is obtained for $x = 1.10$ or $x = x' = \nu' + w$, where ν' and w are the critical exponents of the correlation length at $T < T_\lambda$, and of the velocity of second sound (see Table I). We use $x \equiv x'$ in the following.

We agree with the result $x = 1.1$ reported in Ref. 35 for $X_3 = 0$, but we disagree with their result $x = 1.3$ for $X_3 = 0.36$ and 1 MHz $\leq \omega/2\pi \leq$ 15 MHz.

The next step is a plot of the data for all ω and all X_3 vs $\omega\tau_0 t^{-x}$ with values of τ_0 so that the data for all mixtures, too, collapse onto one curve. The result is shown in Fig. 18. Within deviations of at most $\pm 5\%$ the data points for all ω and X_3, for the investigated ranges, collapse onto a single curve. The deviation of the data points is random without correlation to ω, $\omega\tau$, or X_3. The values of τ_0, giving the best matching of the individual curves, measured at different ω and X_3, are given in Table III [normalized to $\tau_0(X_3 = 0) = 2.01 \times 10^{-2}$ sec]. These values for τ_0 are plotted in Fig. 14, too. Within their errors, the amplitude τ_0 of the characteristic time $\tau = \tau_0 t^{-x}$ determined from the scaling analysis at $T > T_\lambda$ agrees with the values τ_0' determined in Sec. V A from the fit of the relaxation part of the attenuation and dispersion at $T < T_\lambda$. We can conclude that the critical attenuation α_F of first sound at $T > T_\lambda$ in ^{3}He-^{4}He mixtures with $X_3 \leq 0.517$ and for 9 kHz $\leq \omega/2\pi \leq$ 627 kHz can be scaled by Eq. (8) over at least four decades in $\omega\tau$. The attenuation normalized near T_λ or at $\omega\tau = 1$ is a function of $\omega\tau$ only, thus including the dependence on t, ω, and X_3. The concentration dependence of the amplitude of the characteristic time τ as well as its critical exponent which we find for the scaled critical attenuation at $T > T_\lambda$ agree to within the given errors with the amplitude and critical exponent of the relaxation time $\tau' = \xi'/u_2$ at $T < T_\lambda$. Or in other words, the relaxation time τ' which characterizes α_R and D_R in He II is the same which scales the critical attenuation in He I, possibly to within a factor which is independent of t, ω, and X_3. This seems to be one of the most remarkable results of this research. This agreement also supports our belief in the validity of the subtraction procedure described in Sec. V A, at least for our frequency range.

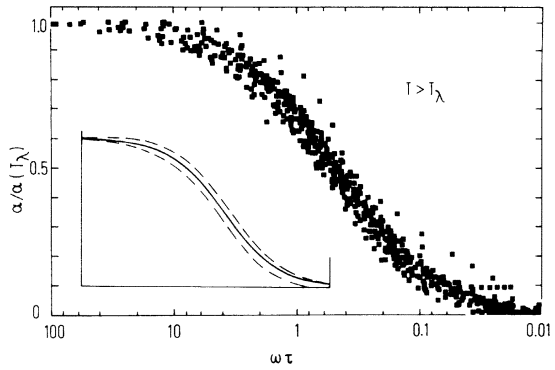

FIG. 18. Scaling plot of the critical attenuation α for $T > T_\lambda$ at 9 kHz $\leq \omega/2\pi \leq$ 627 kHz and for all investigated mixtures versus the scaling variable $\omega\tau$. For $\tau = \tau_0 t^{-x}$ the values for the amplitude and exponent as given in Tables I ($x = x'$) and III are used, which also describe the relaxation attenuation at $T < T_\lambda$. The data are normalized near T_λ. The inset shows as a full line the function $f_F = \omega\tau/(c + \omega\tau)$ with $c = 0.506$. The dashed lines mark the range which includes 95% of our data points.

Because of the smooth behavior of the attenuation data as a function of $\omega\tau$, for all ω and X_3, it is possible to determine the scaling function $f_F(\omega\tau)$. We find that the function

$$f_F(\omega\tau) = \omega\tau/(c + \omega\tau) , \qquad (20)$$

with $c = (0.506 \pm 0.005)$ (τ_0/τ_0') fits the data very well, as shown in Fig. 18. The factor τ_0/τ_0' is necessary, because we obtain only the concentration dependence of τ_0 and not its absolute value from the scaling procedure. The given error for c is one standard deviation; this error in c corresponds to a deviation of the data points in Fig. 18 of about 4% of $\alpha(T_\lambda)$. The same function fits the sound attenuation at the ferromagnetic transition of MnP with $c = 2.2$,[55] and Ahlers[18] has shown that f_F is in agreement with sound attenuation data at 1 GHz for ^{4}He.[38,39]

Equation (20) together with Eq. (8) has an asymptotic behavior for $\omega\tau \ll 1$ which is in disagreement

with the behavior predicted for the hydrodynamic regime [see Eq. (9)], because $y \neq 0$. To remove this inconsistency we fit our data to

$$\bar{f}_F(\omega\tau) = (\omega\tau)^{1-y}/[\bar{c} + (\omega\tau)^{1-y}] . \quad (21)$$

For $X_3 < 0.2$, where $y = 0.1$ (see Fig. 17), our data allow $\bar{f}_F$ and f_F equally well. Because of the required hydrodynamic behavior at $\omega\tau \ll 1$, we prefer $\bar{f}_F$, of course. For the constant in Eq. (21) we find $\bar{c} = (0.55 \pm 0.01)(\tau_0/\tau_0')^{1-y}$ for $X_3 < 0.2$. For the two highest investigated concentrations where $y > 0.1$, our data are better represented by f_F than by $\bar{f}_F$. Possibly, the correct scaling function becomes more complicated at these concentrations.

Figure 18 demonstrates that the scaling function for the attenuation reaches its asymptotic value within the investigated $\omega\tau$ range. Therefore, the exponent of $\omega\tau$ in the numerator and denominator of the scaling function has to be identical, excluding functions like $f_F^* = (\omega\tau)^{1-y}/(c^* + \omega\tau)$.

2. *Dispersion at $T > T_\lambda$*

The dispersion at constant X_3 and t is only very weakly dependent on frequency in the critical region [see Eq. (19) and Fig. 17]. We have therefore plotted D vs $\omega\tau$ for 20 kHz $\leq \omega/2\pi \lesssim$ 600 kHz, $X_3 \leq 0.377$,[57] and at $|T_\lambda^s - T| \geq 5\mu$K. For this plot we used the characteristic time τ determined from the scaling analysis of the attenuation. All data for the four mixtures can be matched if multiplied by $D_0(X_3) = 1$, 1.36, 2.0, and 6.2 for $X_3 = 0$, 0.070, 0.194, and 0.377, respectively. These factors are nearly proportional to τ_0^{-1}. The result, shown in Fig. 19, indicates that D does not approach an asymptotic value in the investigated $\omega\tau$ range but rather increases like $\log_{10}(\omega\tau)$ for $0.4 < \omega\tau < 20$. Multiplying the data in accordance with the analysis of the attenuation by a factor ω^{-y} does not improve the matching of the individual data points.

In an attempt to determine a scaling function for D of similar simplicity as the one found for α, we find that

$$D = D_1(\omega\tau)^2/(d + \omega\tau)^{2-y} , \quad (22)$$

with

$$D_1 = [21.6/D_0(X_3)](\tau_0'/\tau_0)^y \text{ cm/sec} ,$$

$$d = 0.865(\tau_0/\tau_0') ,$$

and $D_0(X_3)$ as mentioned above and y from Fig. 17 represents our data for $0.1 \leq \omega\tau \leq 20$ and $X_3 \leq 0.377$, as shown in Fig. 19. Equation (22) has the predicted frequency dependences at large and small $\omega\tau$. This analysis indicates that the dispersion, too, can be scaled with $\omega\tau$ in the investigated ranges, using the characteristic time τ determined from the behavior of the attenuation.

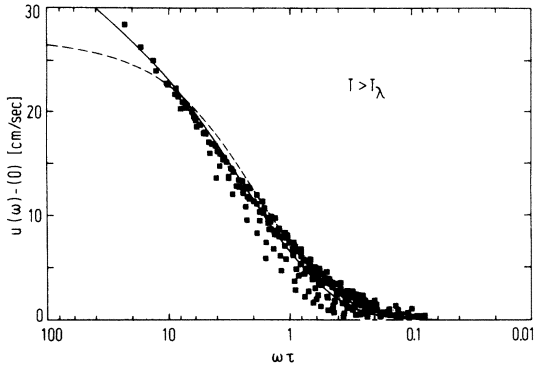

FIG. 19. Scaling plot of the critical dispersion D for $T > T_\lambda$ at 20 kHz $\leq \omega/2\pi \leq$ 627 kHz, $|T_\lambda^s - T| \geq 5\ \mu$K, and for $0 \leq X_3 \leq 0.377$ versus the scaling variable $\omega\tau$. For the characteristic time τ the values deduced from scaling of the attenuation are used. The data for $X_3 = 0$, 0.07, 0.194, and 0.377 are multiplied by $D_0(X_3) = 1$, 1.36, 2.0, and 6.2, respectively. No normalization for the various frequencies is applied. The line is given by Eq. (22) with $y = 0.1$ (see text). For comparison we show the function 27 $[\omega\tau/(0.91 + \omega\tau)]^2$ as a dashed line.

We have no theoretical proof for the above scaling functions and propose them as a representation of our data scaled with $\omega\tau$. The scaling of the attenuation data by Eqs. (20) and (21) is very satisfactory. Scaling the dispersion by Eq. (22) might be questionable for $\omega\tau > 20$, because for large $\omega\tau$ this function diverges.

3. *Attenuation and dispersion at $T < T_\lambda$*

In the analysis we have obtained the following results, which apply for the investigated frequency and concentration ranges:

(i) The critical attenuation (and correspondingly the dispersion) at $T > T_\lambda$ follows Eq. (8) with the scaling function $f_F(\omega\tau)$ or $\bar{f}_F(\omega\tau)$.

(ii) The attenuation and dispersion at $T < T_\lambda$ can be written as a sum of a contribution from an order-parameter relaxation process and a contribution from order-parameter fluctuations. The order-parameter relaxation behaves according to Eqs. (6) if—as our data indicate—the fluctuations contribute about equally at $T > T_\lambda$ and at $T < T_\lambda$. The total attenuation at $T < T_\lambda$ can therefore be written as a sum of Eq. (6) for the relaxation part, and of Eq. (8) with Eq. (20) or Eq. (21) for the fluctuation part. Both processes can be written in a reduced form as functions of $\omega\tau$ with the same characteristic time. But the two scaling functions behave differently; f_R decreases for $\omega\tau > 1$, whereas f_F approaches an asymptotic value at large $\omega\tau$. In addition, the concentration dependence of the strength of the maximum of these two contributions is slightly different, as shown in Fig. 10.

VI. SUMMARY AND CONCLUSIONS

Low-frequency ($\omega/2\pi \lesssim 600$ kHz) measurements of the velocity, of the dispersion, and of the attenuation of first sound have been performed in five ^{3}He-^{4}He mixtures ($X_3 \leq 0.517$) near their λ transitions. From the data at $\omega/2\pi \leq 20$ kHz, the thermodynamic velocity of sound $u(0)$, as well as the related parameters $(\partial S/\partial P)_\lambda$ and $(\partial V/\partial P)_\lambda$ have been determined.

It is shown that for the investigated frequency range attenuation and dispersion near T_λ arise from a relaxation process at $T < T_\lambda$ and from critical fluctuations at $T \lesssim T_\lambda$. The contribution from critical fluctuations seems to be of equal magnitude in the two phases of the mixtures. Both the relaxation and the fluctuation contribution are strongly weakened when the concentration of ^{3}He is increased. The magnitude, temperature, frequency, and concentration dependences of the attenuation and dispersion due to the relaxation process are in agreement with theoretical predictions by Hohenberg[23] and Sanikidze.[25] The obtained relaxation times agree with $\tau' = \xi'/u_2$, using the characteristic length ξ', and the velocity of second sound determined in independent experiments.[26,30,31]

The attenuation and dispersion due to fluctuations at $T > T_\lambda$, for which we do not know a closed-form theoretical prediction, can be scaled with $\omega\tau$ for all investigated ω and X_3, even though they strongly depend on ω and X_3. Scaling functions of $\omega\tau$ which represent the measured attenuation and dispersion are determined. They agree with the expected behavior[34] at small and large $\omega\tau$.

Below T_λ, attenuation and dispersion are the sum of the critical contribution represented by the scaling function and the contribution from order-parameter relaxation. The time τ characterizing the dynamical behavior of the order parameter and determined from the scaling analysis at $T > T_\lambda$ shows the same concentration and temperature dependence as the relaxation time τ' at $T < T_\lambda$; these two times differ at most by a constant factor.

In the critical region for $\omega\tau \gtrsim 1$, attenuation and dispersion behave as $\alpha \sim \omega^{1+y}$, and $D \sim \omega^y$, with $y = 0.10$ for $X_3 < 0.2$, and larger exponents for higher X_3. For $\omega\tau < 0.1$, they allow the expected hydrodynamic ω^2 dependence. The amplitudes of the critical attenuation and of the critical dispersion decrease approximately like the inverse of the amplitude of the characteristic time or of the characteristic length with increasing ^{3}He concentration.

A consistent description of attenuation and dispersion of first sound near T_λ and at $\omega/2\pi \leq 600$ kHz, and their quantitative interpretation is obtained, giving confidence in the applied analysis. A theoretical calculation of the dynamical scaling function and its comparison with our results would be of substantial interest. In addition, a detailed analysis of attenuation data at higher frequencies should be performed. In the frequency range of GHz, e.g., the attenuation seems to behave differently,[37-39] and it might be impossible to apply the analysis discussed in this paper.[35,36] At higher frequencies other processes than the ones considered here will contribute; they will become especially important if the condition $\omega\tau \ll u/u_2$ is violated.[34]

ACKNOWLEDGMENTS

We gratefully acknowledge the cooperation of Dr. W. C. Thomlinson in the early phases of this work, many suggestions concerning experimental problems by Dr. K. H. Mueller, and the assistance of J. Hanssen in the data analysis. We thank Professor K. Kawasaki, Dr. D. Kroll, and Professor H. Wagner for helpful discussions of theoretical questions. We are grateful to Professor H. Meyer for pointing out that his recent investigations indicate that a contribution to α from mass diffusion might be noticeable at our highest ^{3}He concentration.

---

*This work is part of the dissertation of C. Buchal.

[1]G. Ahlers, in *The Physics of Liquid and Solid Helium*, edited by K. H. Bennemann and J. B. Ketterson (Wiley, New York, 1976), Chap. 5.

[2]F. Pobell, in *Proceedings of the European Physical Society Topical Conference, Haifa, 1974*, edited by C. G. Kuper, S. G. Lipson, and M. Revzen (Wiley, New York, 1975).

[3]B. Widom, J. Chem. Phys. 43, 3892 (1965); 43, 3898 (1965); L. P. Kadanoff, Physics 2, 263 (1966); B. D. Josephson, Phys. Lett. 21, 608 (1966).

[4]See, for instance, L. P. Kadanoff, in *Proceedings of the International School, "Enrico Fermi," Course LI*, edited by M. S. Green (Academic, New York, 1971); R. B. Griffiths, Phys. Rev. Lett. 24, 1479 (1970); D. Jasnow and M. Wortis, Phys. Rev. 176, 739 (1968).

[5]See, for instance, K. G. Wilson and J. Kogut, Phys. Rep. 12C, 75 (1974); E. Brézin, D. J. Wallace, and K. G. Wilson, Phys. Rev. B 7, 232 (1973).

[6]K. H. Mueller, F. Pobell, and G. Ahlers, Phys. Rev. Lett. 34, 513 (1975).

[7]C. E. Chase, Phys. Fluids 1, 193 (1958).

[8]M. Barmatz and I. Rudnick, Phys. Rev. 170, 224 (1968).

[9]R. D. Williams and I. Rudnick, Phys. Rev. Lett. 25, 276 (1970); R. D. Williams, thesis (University of California, 1970) (unpublished).

[10]W. C. Thomlinson and F. Pobell, Phys. Rev. Lett. 31, 283 (1973).
[11]T. R. Roberts and S. G. Sydoriak, Phys. Fluids 3, 895 (1960).
[12]M. Barmatz, J. Low Temp. Phys. 5, 419 (1971).
[13]W. C. Thomlinson and F. Pobell, Phys. Lett. A 44, 155 (1973).
[14]E. Brézin, J. C. LeGuillou, and J. Zinn-Justin, Phys. Lett. A 47, 285 (1974).
[15]The highest frequencies used were 591.0, 627.4, 594.3, 598.3, and 606.0 kHz at $X_3=0$, 0.070, 0.194, 0.377, and 0.517, respectively.
[16]Preliminary results for $X_3=0.194$ have been reported in C. Buchal, F. Pobell, and W. C. Thomlinson, Phys. Lett. A 51, 19 (1975).
[17]G. Ahlers, Phys. Rev. 182, 352 (1969).
[18]G. Ahlers, J. Low Temp. Phys. 1, 609 (1969).
[19]A. B. Pippard, Philos. Mag. 1, 473 (1956); M. J. Buckingham and W. M. Fairbank, in *Progress in Low Temperature Physics*, edited by C. J. Gorter (North-Holland, Amsterdam, 1961), Vol. III.
[20]F. Gasparini and M. R. Moldover, Phys. Rev. Lett. 23, 749 (1969); Phys. Rev. B 12, 93 (1975); F. M. Gasparini, thesis (University of Minnesota, 1970) (unpublished); F. M. Gasparini and M. R. Moldover, in *Proceedings of the Thirteenth International Conference on Low Temperature Physics*, edited by K. D. Timmerhaus, W. J. O'Sullivan, and E. F. Hammel (Plenum, New York, 1974), Vol. I.
[21]L. D. Landau and I. M. Khalatnikov, Dokl. Akad. Nauk SSSR 96, 469 (1954).
[22]V. L. Pokrovskii and I. M. Khalatnikov, Zh. Eksp. Teor. Fiz. Pis'ma Red. 9, 225 (1969) [JETP Lett. 9, 149 (1969)]; I. M. Khalatnikov, Zh. Eksp. Teor. Fiz. 57, 489 (1969) [Sov. Phys.-JETP 30, 268 (1970)].
[23]P. C. Hohenberg, in *Proceedings of the International School "Enrico Fermi," Course LI*, edited by M. S. Green (Academic, New York, 1971); we neglect a constant, unknown factor of order unity in Eq. (4.13) of this reference [corresponding to our Eq. (3)].
[24]G. Ahlers, Phys. Rev. A 3, 696 (1971); 8, 530 (1972).
[25]D. G. Sanikidze, Zh. Eksp. Teor. Fiz. 66, 714 (1974) [Sov. Phys.-JETP 39, 345 (1974)]; a square is missing on $(\partial S/\partial P)_\lambda$ in the last term of Eq. (24) in this reference.
[26]G. Ahlers, Phys. Rev. A 10, 1670 (1974).
[27]R. A. Ferrell, N. Menyhard, H. Schmidt, F. Schwabl, and P. Szepfalusy, Ann. Phys. (N.Y.) 47, 565 (1968).
[28]B. I. Halperin and P. C. Hohenberg, Phys. Rev. Lett. 19, 700 (1967); Phys. Rev. 177, 952 (1969).
[29]B. I. Halperin, P. C. Hohenberg, and E. D. Siggia, Phys. Rev. B 13, 1299 (1976).
[30]G. G. Ihas and F. Pobell, Phys. Rev. A 9, 1278 (1974).
[31]W. C. Thomlinson, G. G. Ihas, and F. Pobell, Phys. Rev. Lett. 31, 1284 (1973); Phys. Rev. B 11, 4292 (1975).
[32]We don't use the scaling law $3\nu'-2=-\alpha'$ at this point because values for $3\nu'-2$ (Ref. 31) and $-\alpha'$ (Refs. 20 and 26) measured at constant P and X_3 don't agree for the mixtures. For pure ^{4}He this scaling law is very well fulfilled, giving $3\nu'-2=-\alpha'=0.026$ (Ref. 6). For the mixtures, universality has only been proven for ν' (and ζ) at $X_3<0.4$ (Refs. 26 and 31).
[33]J. Swift and L. P. Kadanoff, Ann. Phys. (N.Y.) 50, 312 (1968).
[34]K. Kawasaki, Phys. Lett. A 31, 165 (1970); Int. J. Magn. 1, 171 (1971); and private communication.
[35]A. Ikushima, D. B. Roe, and H. Meyer, in *Proceedings of the Second International Conference on Phonon Scattering in Solids*, edited by L. J. Challis, V. W. Rampton, and A. F. G. Wyatt (Plenum, New York, 1976).
[36]A. Ikushima and K. Tozaki, in *Proceedings of the Fourteenth International Conference on Low Temperature Physics*, edited by M. Krusius and M. Vuorio (North-Holland, New York, 1975), Vol. I.
[37]J. M. Vaughan, W. F. Vinen, and C. J. Palin, in *Proceedings of the Thirteenth International Conference on Low Temperature Physics*, edited by K. D. Timmerhaus, W. J. O'Sullivan, and E. F. Hammel (Plenum, New York, 1974), Vol. I; G. Winterling, F. S. Holmes, and T. J. Greytak, *ibid.* Vol. I; Phys. Rev. Lett. 30, 427 (1973).
[38]W. Heinicke, G. Winterling, and K. Dransfeld, Phys. Rev. Lett. 22, 170 (1969); J. S. Imai and I. Rudnick, *ibid.* 22, 694 (1969).
[39]D. E. Commins and I. Rudnick, in *Proceedings of the Thirteenth International Conference on Low Temperature Physics*, edited by K. D. Timmerhaus, W. J. O'Sullivan, and E. F. Hammel (Plenum, New York, 1974), Vol. I.
[40]L. E. DeLong, O. G. Symko, and J. C. Wheatley, Rev. Sci. Instrum. 42, 147 (1971).
[41]Model CR 2500 L, Cryo. Cal. Inc., Riviera Beach, Fla.
[42]G. Ahlers, Phys. Rev. 171, 275 (1968).
[43]H. Kojima, W. Veith, S. J. Putterman, E. Guyon, and I. Rudnick, Phys. Rev. Lett. 27, 714 (1971).
[44]F. G. Brickwedde *et al.*, J. Res. Natl. Bur. Stand. (U.S.) A 64, 1 (1960).
[45]G. Ahlers, Phys. Rev. Lett. 24, 1333 (1970).
[46]H. A. Kierstaedt, Phys. Rev. 162, 153 (1967).
[47]T. Satoh and A. Kakizaki, in *Proceedings of the Thirteenth International Conference on Low Temperature Physics*, edited by K. D. Timmerhaus, W. J. O'Sullivan, and H. F. Hammel (Plenum, New York, 1974), Vol. I.
[48]E. C. Kerr, in *Low Temperature Physics and Chemistry*, edited by J. R. Dillinger (University of Wisconsin Press, Madison, 1958); E. C. Kerr and R. D. Taylor, Ann. Phys. (N.Y.) 26, 292 (1964).
[49]A tabulation of smoothed velocity, dispersion, and attenuation data for all investigated frequencies and mixtures as well as further detailed results from the various fits can be found in C. Buchal, thesis, JÜL report (unpublished).
[50]N. E. Dyumin, B. N. Eselson, and E. Y. Rudavskij, Ukr. Fiz. Zh. 19, 818 (1974).
[51]In this section, equations are only written down for attenuation; the analog equations for dispersion are obvious. The analysis has been performed for both, of course.
[52]There seems to be a slight tendency towards $q>1.0$, which would mean $\zeta_0'/\zeta_0>1.0$. Very recently $\zeta_0'/\zeta_0\simeq 2.4$ has been calculated for ^{4}He (Ref. 29).
[53]In the original analysis of the data of Ref. 9 the incorrect assumptions $\Delta u=\text{const}$, $\alpha=\alpha_{R,\max}$ at $\omega\tau'=1$, as well as the constraint $\zeta'\sim(T_\lambda-T)^{-2/3}$ were applied.
[54]For this determination our data were weighted according to our confidence in them as follows: attenuation at

600 kHz: 3; at 200 kHz and at 100 kHz: 2; at 40 kHz and at 20 kHz: 1; below 20 kHz: 0. Dispersion at 600 kHz: 3; at 200 kHz: 2; at 100 kHz: 1; below 50 kHz: 0.

[55]B. Golding, Phys. Rev. Lett. 34, 1102 (1975).

[56]The same exponents y as for $\alpha(T \simeq T_\lambda) \sim \omega^{1+y}$ are found for $\alpha^+(\omega\tau = 1) \sim \omega^{1+y}$.

[57]In the scaling analysis of the dispersion we excluded the data for $X_3 = 0.517$ because of their small values, and resulting significant scatter.